



저작자표시-비영리-변경금지 2.0 대한민국

이용자는 아래의 조건을 따르는 경우에 한하여 자유롭게

- 이 저작물을 복제, 배포, 전송, 전시, 공연 및 방송할 수 있습니다.

다음과 같은 조건을 따라야 합니다:



저작자표시. 귀하는 원저작자를 표시하여야 합니다.



비영리. 귀하는 이 저작물을 영리 목적으로 이용할 수 없습니다.



변경금지. 귀하는 이 저작물을 개작, 변형 또는 가공할 수 없습니다.

- 귀하는, 이 저작물의 재이용이나 배포의 경우, 이 저작물에 적용된 이용허락조건을 명확하게 나타내어야 합니다.
- 저작권자로부터 별도의 허가를 받으면 이러한 조건들은 적용되지 않습니다.

저작권법에 따른 이용자의 권리는 위의 내용에 의하여 영향을 받지 않습니다.

이것은 [이용허락규약\(Legal Code\)](#)을 이해하기 쉽게 요약한 것입니다.

[Disclaimer](#)

Thesis for the Degree of Master of Engineering

Finite Element Analysis of EMI
Signatures of Damaged Structural
Connection via High-Performance
Interface Washer



by

Nguyen Khac Duy

Department of Ocean Engineering

The Graduate School

Pukyong National University

February 2011

Finite Element Analysis of EMI Signatures of Damaged Structural Connection via High-Performance Interface Washer



A thesis submitted in partial fulfillment of the requirements
for the degree of
Master of Engineering

in Department of Ocean Engineering, the Graduate School,
Pukyong National University
February 2011

Nguyen Khac Duy의 공학석사 학위논문을 인준함

2010년 12월 17일



주 심 공학박사 류 연 선 (인)
위 원 공학박사 나 원 배 (인)
위 원 공학박사 김 정 태 (인)

TABLE OF CONTENTS

TABLE OF CONTENTS	i
LIST OF FIGURES	iv
LIST OF TABLES	vi
ABSTRACT	vii
CHAPTER 1 INTRODUCTION	1
1.1 Background	1
1.2 Objective and Scope.....	3
1.3 Organization of the Thesis.....	4
CHAPTER 2 IMPEDANCE-BASED SHM	5
2.1 Introduction	5
2.2 Piezoelectric Constitutive Relations.....	5
2.3 Electro-Mechanical Impedance	7
2.4 Approaches for Damage Evaluation	8
2.4.1 Frequency Shift and Impedance Amplitude Change	8
2.4.2 Root Mean Square Deviation	9
2.4.3 Mean Absolute Percentage Deviation	9
2.4.4 Correlation Coefficient Deviation	10
CHAPTER 3 FEASIBILITY OF FE ANALYSIS OF EM IMPEDANCE	11
3.1 Introduction	11
3.2 EM Impedance Analysis for a Free-Free Beam	11

3.3 EM Impedance Analysis for a Cantilever Beam	15
CHAPTER 4 INTERFACE WASHER FOR STRUCTURAL CONNECTION MONITORING	17
4.1 Introduction	17
4.2 Issues of Conventional Impedance-Based Method	17
4.3 Interface Washer for Compressive Force Monitoring	18
4.3.1 Description of Interface Washer	18
4.3.1 Advantages of Interface Washer	20
CHAPTER 5 FE ANALYSIS OF EM IMPEDANCE FOR CABLE-ANCHOR CONNECTION	24
5.1 Introduction	24
5.2 FE Analysis of EM Impedance for Cable-Anchor Connection	24
5.2.1 Description of FE Model	24
5.2.2 Static-Dynamic Coupled Impedance Analysis	29
5.2.3 Effect of Anchor Force on EM Impedance Signature	30
5.3 Experimental Verification for Cable-Anchor Connection	34
5.4 Design of Interface Washer	37
5.4.1 Effect of Material Properties of Interface Washer on EM Impedance Signature	37
5.4.2 Effect of Geometrical Properties of Interface Washer on EM Impedance Signature	39
CHAPTER 6 FE ANALYSIS OF EM IMPEDANCE FOR BOLTED CONNECTION	42
6.1 Introduction	42
6.2 FE Analysis of EM Impedance for Bolted Connection	42
6.2.1 Description of FE Model	42
6.2.2 Effect of Bolt Loosening on EM Impedance Signature	44
6.3 Experimental Verification for Bolted Connection	47

CHAPTER 7 CONCLUSIONS.....50

REFERENCE52



LIST OF FIGURES

Figure 2.1	1-D model electro-mechanical interaction between piezoelectric patch and host structure (Liang, 1996)	8
Figure 3.1	Experimental specimen (Giugliuti and Zagrai, 2002)	12
Figure 3.2	Geometry of free-free beam	12
Figure 3.3	FE model of free-free beam	13
Figure 3.4	Impedance signatures of free-free beam.....	14
Figure 3.5	Experimental setup of cantilever beam.....	15
Figure 3.6	Geometry of cantilever beam (Unit: mm).....	16
Figure 3.7	FE model of cantilever beam.....	16
Figure 3.8	Impedance signatures of cantilever beam.....	16
Figure 4.1	Interface washer for compressive force monitoring.....	19
Figure 4.2	Installed interface washer in cable-anchor connection.....	20
Figure 4.3	FE model of cable anchor connection without interface washer (model A).....	21
Figure 4.4	FE model of cable-anchor connection with interface washer (model B).....	22
Figure 4.5	Impedance signatures for model A.....	22
Figure 4.6	Impedance signatures for model B.....	23
Figure 4.7	RMSD indices for two models A and B.....	23
Figure 5.1	Experimental setup of cable-anchor connection.....	26
Figure 5.2	Experimental impedance signatures in frequency range of 30 kHz – 40 kHz.....	26
Figure 5.3	Experimental impedance signatures in frequency range of 60 kHz – 70 kHz.....	27
Figure 5.4	Experimental impedance signatures in frequency range of 10 kHz – 100 kHz.....	27
Figure 5.5	RMSD indices for various frequency ranges (Experiment)...	28
Figure 5.6	FE model of cable-anchor connection.....	28
Figure 5.7	Static-dynamic coupled impedance analysis.....	30

Figure 5.8	Deformations of cable-anchor connection at 36.16 kHz.....	31
Figure 5.9	Numerical impedance signatures for various anchor forces...	32
Figure 5.10	Impedance Real values at 36.16 kHz (FE analysis).....	33
Figure 5.11	Statistical damage indices due to loss of anchor force (FE analysis)	33
Figure 5.12	Experimental impedance signatures for various anchor forces.....	35
Figure 5.13	Resonance impedance and frequency shift results (Experiment).....	36
Figure 5.14	Statistical damage indices due to loss of anchor force (Experiment).....	36
Figure 5.15	Numerical impedance signatures of cable anchor connection with steel interface washer.....	38
Figure 5.16	Comparison of RMSD indices by using aluminum and steel interface washers (FE analysis).....	39
Figure 5.17	Numerical impedance signatures for various thicknesses of interface washer under anchor force of 79.5 kN.....	40
Figure 5.18	RMSD indices for 8.64% loss of anchor force by using interface washers with various thicknesses (FE analysis).....	41
Figure 6.1	Experimental setup of bolted connection.....	43
Figure 6.2	FE model of bolted connection.....	44
Figure 6.3	Deformations of bolted connection at 36 kHz.....	45
Figure 6.4	Numerical impedance signatures for models M1 and M2.....	46
Figure 6.5	Numerical impedance signatures for models M1 and M3.....	46
Figure 6.6	RMSD indices for two damaged models M2 and M3 (FE analysis).....	47
Figure 6.7	Experimental impedance signatures for undamaged and Bolt 1 loosened states.....	48
Figure 6.8	Experimental impedance signatures for undamaged and Bolt 2 loosened states.....	48
Figure 6.9	RMSD indices for two damaged cases (Experiment).....	49

LIST OF TABLES

Table 3.1	Material properties of PZT-5A	13
Table 3.2	Resonance frequencies from experimental, theoretical and FE analysis	14
Table 4.1	Material properties of interface washer	19
Table 5.1	Material properties of anchor plate and anchorage	29
Table 6.1	Bolt loosening scenarios	44



Finite Element Analysis of EMI Signatures of Damaged Structural Connection via High-Performance Interface Washer

Nguyen Khac Duy

Department of Ocean Engineering
The Graduate School
Pukyong National University

ABSTRACT

Structural connections are important parts of most infrastructures since the failure of the connections can lead to the loss of serviceability and structural collapse. Therefore, damage detection on structural connections has become an important topic. Among many technologies, impedance-based method has been found very promising for monitoring small incipient damage in critical members like structural connections. This study presents a finite element analysis of electro-mechanical impedance (EMI) signatures of damaged structural connections via a high-performance interface washer. To achieve the objective, the following approaches are implemented. Firstly, an interface washer is designed to monitor the changes in stress fields. The interface washer is a thin plate which is installed in structural connection. On the interface washer, a piezoelectric (PZT) patch is attached to monitor the changes in structural impedance by changes in stress fields. Secondly, a finite element model of structural connection such as cable anchor connection and bolted connection is established. In the finite element analysis, the interface washer is modeled to represent changes in stress

fields on the connection by using impedance-based method. Also, the effects of material and geometrical properties of the interface washer on EMI signatures are examined to aim at designing the optimal interface washer. Thirdly, the feasibility of the finite element analysis is validated by experiments on a lab-scale cable anchor connection and a bolted connection.



CHAPTER 1

INTRODUCTION

1.1 Background

Structural connection such as bolted connection and cable-anchor connection is the important part of most infrastructures. Cable-anchor connection is usually observed in prestressed concrete bridge, cable-stayed bridge, and suspension bridge. Meanwhile, bolted connection is much found in steel structures like steel bridge, pipeline system, and tower. These structures usually cost a huge amount of expense and contribute the important roles to living, transportation, industry as well as economics. However, members with structural connections are usually weak parts and much influenced by severe loading and environmental conditions. Moreover, structural connections themselves have potential damage types such as relaxation in connection components, reduction of stress fields, and fatigue cracks in bolt holes. These damages could cause failure of structural connection, reduction of load carrying capacity and so far lead to severe disasters. Therefore, structural health monitoring (SHM) on structural connection becomes a key issue to ensure the safety and serviceability of a structure.

Related to SHM, there are two large branches as global SHM and local SHM. Up to date, many studies have been focused on SHM of structural connections by using global and local dynamic characteristics (Lam et al., 1998; Yun et al., 2001; Kim et al., 2006a; Fasel et al., 2005; Park et al., 2005; Mascarenas et al., 2007; Kim et al., 2008; Kim et al., 2009; Kim et al., 2010). The global SHM which usually deals with acceleration-based methods can monitor the structural integrity with several distributed sensors. However, acceleration-based methods are not very sensitive to local incipient damage since these methods employ the low frequency responses which have the long wave-lengths. On the other hand, impedance-based local SHM is found to be very promising to capture small damage at limited

region like cable-anchor connection or bolted connection.

The impedance-based method was first proposed by Liang et al. (1996). Since then, many researchers have improved the method and applied the method to various damage detection problems. To deal with this method, a piezoelectric material is usually surface-bonded on the structural region needed to monitor. The most commonly available form of piezoelectric material is the Lead Zirconate Titanate (PZT). The PZT patch is deformed due to an electric field applied on PZT. The deformation of PZT then causes the deformation of structure. As the inverse effect, an electric field is produced when the PZT patch is subjected to mechanical strain from host structure. These properties allow the PZT patch work both as actuator and sensor.

The basic concept of the impedance-based method is to monitor the variation of electric impedance of piezoelectric sensor in high frequency band by employing the electro-mechanical coupling property of piezoelectric materials. The frequency range dealt with impedance-based method is typically higher than 30 kHz. Because of the high-frequency range employed, the method is very sensitive to incipient damage in a structure (Park et al., 2003). Moreover, the short wave-length associated with the high frequency band allows this method capture dynamic response of local critical member.

The advantages of this method are its capability of capturing a wide range of structural damage from small to large scale, availability of continuous online monitoring, practical applicability and cost-effectiveness (Tseng et al, 2005). According to its features, the impedance-based method has been successfully implemented to various structures, e.g., a massive steel bridge joints (Ayres et al., 1998), a bonded composite structure (Koh et al., 1999), a prototype reinforced concrete bridge (Soh et al., 2000), pipeline systems (Park et al., 2001), thin circular plates (Zagrai and Giugliutiu, 2001), aircraft turbo-engine blades (Giugliutiu and Zagrai, 2002), aluminum strips and plates (Tseng and Naidu, 2002), concrete beam and frame (Park et al.,

2006; Bhalla et al., 2003; Yang et al., 2008), bolted connection (Mascarenas et al., 2007), plate girder bridge (Kim et al., 2006b), and cable anchor connection (Kim et al., 2010; Park et al., 2010a; Park et al., 2010c).

Beside the above-mentioned advantages, the behavior of electro-mechanical impedance due to damages has not been clearly identified. Numerical study, therefore, has obtained its demands for interesting topic. Many efforts on simulation of electro-mechanical impedance responses were carried out by many researchers. Giugliuti and Zagari (2002) established a numerical simulation of electro-mechanical impedance for a free-free aluminum beam with consideration of different thicknesses and widths of the beam. Park et al. (2006) examined effects of multiple cracks in concrete beam on electro-mechanical impedance signatures by using finite element (FE) analysis. In these numerical studies, however, the dynamics properties of structures without external force effect were considered. For cable-anchor and bolted connections, the loss of pressure is the main damage. To monitor the pressure loss, the effect of pressure on dynamic characteristic should be included. In this study, this effect will be considered when analyzing the electro-mechanical impedance of structural connections.

1.2 Objective and Scope

The objective of this study is to establish a FE analysis of electro-mechanical impedance signatures of damaged structural connections via a high-performance interface washer. In order to achieve the goal, the following tasks are performed:

1. An interface washer is designed to monitor changes in stress fields. The interface washer is a thin plate which is installed in structural connection. On the interface washer, a piezoelectric (PZT) patch is attached to monitor the changes in structural impedance by changes in stress fields.
2. An FE model of structural connection such as cable anchor connection and bolted connection is established. In the FE

- analysis, the interface washer is modeled to represent changes in stress fields on the connection by using impedance-based method.
3. The effects of material and geometrical properties of the interface washer on impedance signatures are examined to aim at designing the optimal interface washer.
 4. The feasibility of the FE analysis is validated by lab-scale cable anchor connection and bolted connection models.

1.3 Organization of the Thesis

The remaining of the work is divided into 5 chapters. In Chapter 2, the impedance-based method is reviewed. The electro-mechanical impedance is presented as the combination of mechanical impedance of structure and mechanical impedance of piezoelectric material. Several methods to monitor the impedance signatures are summarized. In Chapter 3, the feasibility of FE analysis of electro-mechanical impedance is evaluated by simple models as free-free beam and cantilever beam. In Chapter 4, an interface washer is introduced to monitor the compressive force in structural connection. The advantages of using interface washer on impedance-based method are also pointed out. In Chapter 5, the FE analysis of electro-mechanical impedance for cable-anchor connection with using interface washer is performed. For FE model, by using static-dynamic coupled impedance analysis method, the effect of anchor force on impedance signature can be investigated. An experiment on lab-scale cable-anchor connection is carried out to verify the FE analysis results. In Chapter 6, the FE analysis of electro-mechanical impedance for bolted connection with using interface washer is performed. The effect of bolt loosening on electro-mechanical impedance signature is evaluated by numerical study. An experiment on lab-scale bolted connection is carried out to verify the right of numerical results. Finally, Chapter 7 summarizes the research details of this thesis, and future researches on impedance-based method using FE analysis.

CHAPTER 2

IMPEDANCE-BASED METHOD

2.1 Introduction

In this chapter, the basic background of impedance-based method is outlined. Firstly, the constitutive equations of piezoelectric material are presented as the couple relation of mechanical and electrical properties. Secondly, electro-mechanical impedance of structure coupled with piezoelectric material is illustrated. Finally, some approaches to monitor the electro-mechanical impedance signatures are considered.

2.2 Piezoelectric Constitutive Relations

The constitutive equations in strain-charge relation for a piezoelectric material can be expressed by tensor form as:

$$\begin{aligned} S_{ij} &= s_{ijkl}^E T_{kl} + d_{kij} E_k \\ D_j &= d_{jkl} T_{kl} + \varepsilon_{jk}^T E_k \end{aligned} \quad (2.1)$$

where S_{ij} is strain vector; s_{ijkl}^E is elastic compliance of the piezoelectric material at zero electric field ($E_k = 0$); E_k is electric field vector; T_{kl} is stress vector; d_{jkl} is piezoelectric coupling constant; D_j is electrical displacement; and ε_{jk}^T is dielectric permittivity at zero mechanical stress ($T_{kl} = 0$). These parameters can be expressed as follows:

$$S_{ij} = \begin{pmatrix} S_{11} \\ S_{22} \\ S_{33} \\ S_{23} \\ S_{31} \\ S_{12} \end{pmatrix} \quad (2.2a); \quad T_{kl} = \begin{pmatrix} T_{11} \\ T_{22} \\ T_{33} \\ T_{23} \\ T_{31} \\ T_{12} \end{pmatrix} \text{ (N/m}^2\text{)} \quad (2.2b)$$

$$s_{ijkl}^E = \begin{pmatrix} s_{11}^E & s_{12}^E & s_{13}^E & 0 & 0 & 0 \\ s_{21}^E & s_{22}^E & s_{23}^E & 0 & 0 & 0 \\ s_{31}^E & s_{32}^E & s_{33}^E & 0 & 0 & 0 \\ 0 & 0 & 0 & s_{44}^E & 0 & 0 \\ 0 & 0 & 0 & 0 & s_{55}^E & 0 \\ 0 & 0 & 0 & 0 & 0 & s_{66}^E \end{pmatrix} \text{ (m}^2\text{/N)} \quad (2.2c)$$

$$d_{kij} = \begin{pmatrix} 0 & 0 & d_{31} \\ 0 & 0 & d_{32} \\ 0 & 0 & d_{33} \\ 0 & d_{24} & 0 \\ d_{15} & 0 & 0 \\ 0 & 0 & 0 \end{pmatrix} \text{ (C/N or m/V)} \quad (2.2d)$$

$$E_k = \begin{pmatrix} E_1 \\ E_2 \\ E_3 \end{pmatrix} \text{ (V/m)} \quad (2.2e); \quad D_j = \begin{pmatrix} D_1 \\ D_2 \\ D_3 \end{pmatrix} \text{ (C/m}^2\text{)} \quad (2.2f)$$

$$\varepsilon_{jk}^T = \begin{pmatrix} \varepsilon_{11} & 0 & 0 \\ 0 & \varepsilon_{22} & 0 \\ 0 & 0 & \varepsilon_{33} \end{pmatrix} \text{ (Farad/m)} \quad (2.2g)$$

From the constitutive equations, the piezoelectric material strains when an electric field is applied to the piezoelectric material, or produces an electric field when the piezoelectric material is strained as the inverse effect.

2.3 Electro-Mechanical Impedance

The impedance-based method is based on the coupling of mechanical and electrical features (Liang et al., 1996). In this method, a piezoelectric patch is usually surface-bonded to a host structure. The electrical effect of piezoelectric is partly controlled by mechanical effect of host structure. As shown in Fig. 2.1, the interaction between the piezoelectric patch and the host structure is conceptually explained as an idealized 1-D electro-mechanical relation. The host structure is described as the effects of mass, stiffness, damping, and boundary condition. The PZT patch is modeled as a short circuit powered by a harmonic voltage or current. The electro-mechanical (EM) impedance $Z(\omega)$ which is generated from the PZT patch is a combined function of the mechanical impedance of the host structure, $Z_s(\omega)$, and that of the piezoelectric patch, $Z_a(\omega)$, as follows:

$$Z(\omega) = \left\{ i\omega \frac{wl}{t_c} \left[\left(\varepsilon_{33}^T - d_{3x}^2 \hat{Y}_{xx}^E \right) + \frac{Z_s(\omega)}{Z_a(\omega) + Z_s(\omega)} d_{3x}^2 Y_{xx}^E \left(\frac{\tan kl}{kl} \right) \right] \right\}^{-1} \quad (2.3)$$

where, $\hat{Y}_{xx}^E = (1 + j\eta)Y_{xx}^E$ is the complex Young's modulus of the PZT patch at zero electric field where $Y^E = [s^E]^{-1}$; $\hat{\varepsilon}_{xx}^T = (1 - j\delta)\varepsilon_{xx}^T$ is the complex dielectric constant at zero stress; d_{3x} is the piezoelectric coupling constant in x -direction at zero stress; $k = \omega\sqrt{\rho/\hat{Y}_{xx}^E}$ is the wave number where ρ is the mass density of the structure; and w , l , and t_c are the width, length, and thickness of the piezoelectric transducer, respectively. The parameters η and δ are structural damping loss factor and dielectric loss factor of piezoelectric material, respectively. In Eq. (2.3), the mechanical impedance of the host structure $Z_s(\omega)$ is the ratio of PZT force to structural velocity at PZT location, as follows:

$$Z_s(\omega) = \frac{f_{PZT}}{\dot{x}_{PZT}} = \frac{F_{PZT}e^{i\omega t}}{\dot{x}_{PZT}} \quad (2.4)$$

If the structure is considered as a system of single degree of freedom, the mechanical impedance of the host structure can be expressed as:

$$Z_s(\omega) = m\omega j + c - \frac{k}{\omega} j \quad (2.5)$$

Equation (2.5) shows that the mechanical impedance of the host structure is a function of mass, damping and stiffness. Therefore, any changes in dynamic characteristics of the structure could be represented in the change in EM impedance.

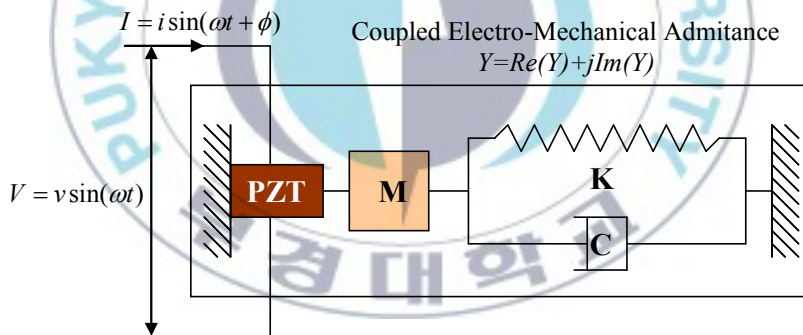


Figure 2.1 1-D model electro-mechanical interaction between piezoelectric patch and host structure (Liang, 1996)

2.4 Approaches of Damage Evaluation

Assume that when damage occurs on the structure, mechanical and electrical properties of the PZT patch are not changed. The change in EM impedance only represents the changes in structural impedance. To evaluate the change in EM impedance, we can monitor the shift of frequency, the change in impedance amplitude at resonance, root mean square deviation

index, mean absolute percentage deviation and correlation coefficient deviation.

2.4.1 Frequency Shift and Impedance Amplitude Change

Generally, the peak of impedance is very sensitive to the change in structural properties. Therefore, the change in structural impedance can be monitored by the change in frequency shift and impedance peak amplitude. Generally, resonant frequency increases when structural stiffness increases, or mass decreases. Meanwhile, resonant amplitude increases when structural damping decreases.

2.4.2 Root Mean Square Deviation

To quantify the change of impedance signature in a frequency range, Sun et al. (1995) used the root mean square deviation (RMSD) of impedance signatures measured before and after the occurrence of damage. RMSD index is calculated based on the following equation:

$$RMSD = \sqrt{\frac{\sum_{i=1}^n [\text{Re}(Z^*(\omega_i)) - \text{Re}(Z(\omega_i))]^2}{\sum_{i=1}^n [\text{Re}(Z(\omega_i))]^2}} \quad (2.6)$$

where $\text{Re}(Z(\omega_i))$ and $\text{Re}(Z^*(\omega_i))$ are the real parts of the impedance signatures of the i^{th} frequency measured before and after damage occurrence, respectively. Also, n signifies the number of frequency points in the sweep band.

2.4.3 Mean Absolute Percentage Deviation

Zagrai and Giurgiutiu (2001) used another statistical method as mean absolute percentage deviation (MAPD) to quantify the change of impedance signatures due to damage. MAPD index is calculated based on the following equation:

$$MAPD = \frac{1}{n} \sum_{i=1}^n \left| \frac{[\text{Re}(Z^*(\omega_i)) - \text{Re}(Z(\omega_i))]}{[\text{Re}(Z(\omega_i))]} \right| \quad (2.7)$$

2.4.4 Correlation Coefficient Deviation

The correlation coefficient deviation (CCD) can also be used to quantify the change of impedance signature due to damage in a whole frequency range (Zagrai and Giurgiutiu, 2001). CCD index is calculated as follows:

$$CCD = 1 - CC \quad (2.8)$$

and

$$CC = \frac{1}{\sigma_Z \sigma_Z^*} E \left\{ [\text{Re}(Z_i) - \text{Re}(\bar{Z})][\text{Re}(Z_i^*) - \text{Re}(\bar{Z}^*)] \right\} \quad (2.9)$$

where σ_Z and σ_Z^* signify the standard deviation of impedance signatures before and after damage; \bar{Z} and \bar{Z}^* signify the mean value of impedance signatures before and after damage.

CHAPTER 3

FEASIBILITY OF FE ANALYSIS OF EM IMPEDANCE

3.1 Introduction

To evaluate the performance of FE analysis of EM impedance, FE models of two simple structures are carried out. Firstly, an FE model of a free-free aluminum beam which was used in a published study (Giurgiutiu and Zagrai, 2002) is established. EM impedance of the aluminum beam from the FE analysis will be compared with experimental results. Secondly, FE analysis of EM impedance of a cantilever beam is performed. Also, an experiment on cantilever beam is carried out to verify the FE analysis' result.

3.2 EM Impedance Analysis for a Free-Free Beam

To evaluate the performance of FE analysis method, a model of a free-free beam which was studied by Giurgiutiu and Zagrai (2002) is established. The free-free beam is shown in Fig. 3.1. That was a small thin steel beam with length as 100mm, width as 8 mm, and thickness as 2.6 mm. Material properties of the steel beam are as follows: Young's modulus, $E = 200$ GPa, mass density, $\rho = 7750$ kg/m³, and mechanical loss factor, $\eta = 0.02$. A PZT patch with 7x7x0.22 mm size was attached at 40 mm distant from the left edge of the beam. Assuming the PZT patch used in that study is PZT-5A type, material properties of PZT patch are outlined in Table 3.1 (eFunda Inc, 2010). In Table 3.1, the elastic compliance, dielectric coupling constant and permittivity of the PZT patch are previously described in Eqs.(2.2c), (2.2d) and (2.2g), respectively.

The detailed geometries of the beam and the PZT patch are given in Fig. 3.2. According to the specimen of Giurgiutiu and Zagrai (2002), an FE model is established using COMSOL 3.4 software (COMSOL, 2010) as shown in Fig. 3.3. The EM impedance is then calculated by FE analysis. Figure 3.4 shows the comparison of impedance signatures between the experimental (and theoretical) results carried out by Giurgiutiu and Zagrai

(2002) and the FE analysis result of this study. The FE results show the good matching with experimental and theoretical ones. The resonances are well presented by FE analysis. The resonance frequencies from experimental, theoretical results and FE analysis are outlined in Table 3.2. As shown in Table 3.2, the small errors of peak frequencies are obtained. It is worth noting that the amplitudes at resonances are much dependent on damping value which is unknown. The gap between the experimental line and the FE line may be caused by inaccuracy of PZT type which was not considered by Giurgiutiu and Zagrai (2002).



Figure 3.1 Experimental specimen (Giurgiutiu and Zagrai, 2002)

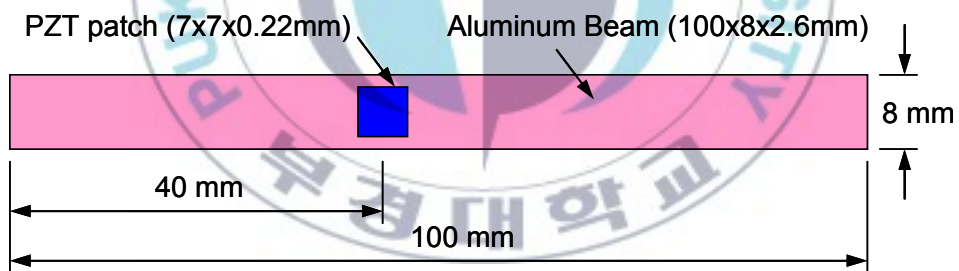


Figure 3.2 Geometry of free-free beam

Table 3.1 Material properties of PZT-5A

Quantity	Value
Elastic compliance, s_{ijkl}^E (m ² /N)	$\begin{pmatrix} 16.4 & -5.74 & -7.22 & 0 & 0 & 0 \\ -5.74 & 16.4 & -7.22 & 0 & 0 & 0 \\ -7.22 & -7.22 & 18.8 & 0 & 0 & 0 \\ 0 & 0 & 0 & 47.5 & 0 & 0 \\ 0 & 0 & 0 & 0 & 47.5 & 0 \\ 0 & 0 & 0 & 0 & 0 & 44.3 \end{pmatrix} \times 10^{-12}$
Dielectric coupling constant, d_{kij} (C/N)	$\begin{pmatrix} 0 & 0 & -171 \\ 0 & 0 & -171 \\ 0 & 0 & 374 \\ 0 & 584 & 0 \\ 584 & 0 & 0 \\ 0 & 0 & 0 \end{pmatrix} \times 10^{-12}$
Permittivity, ϵ_{jk}^T (Farad/m)	$\begin{pmatrix} 1730 & 0 & 0 \\ 0 & 1730 & 0 \\ 0 & 0 & 1700 \end{pmatrix} \times (8.854 \times 10^{-12})$
Mass density, ρ (kg/m ³)	7750
Damping loss factor, η	0.0125
Dielectric loss factor, δ	0.015

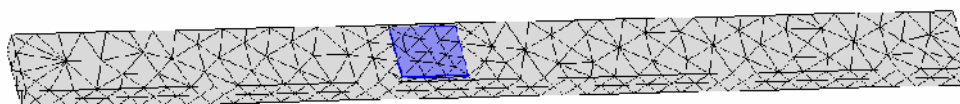


Figure 3.3 FE model of free-free beam

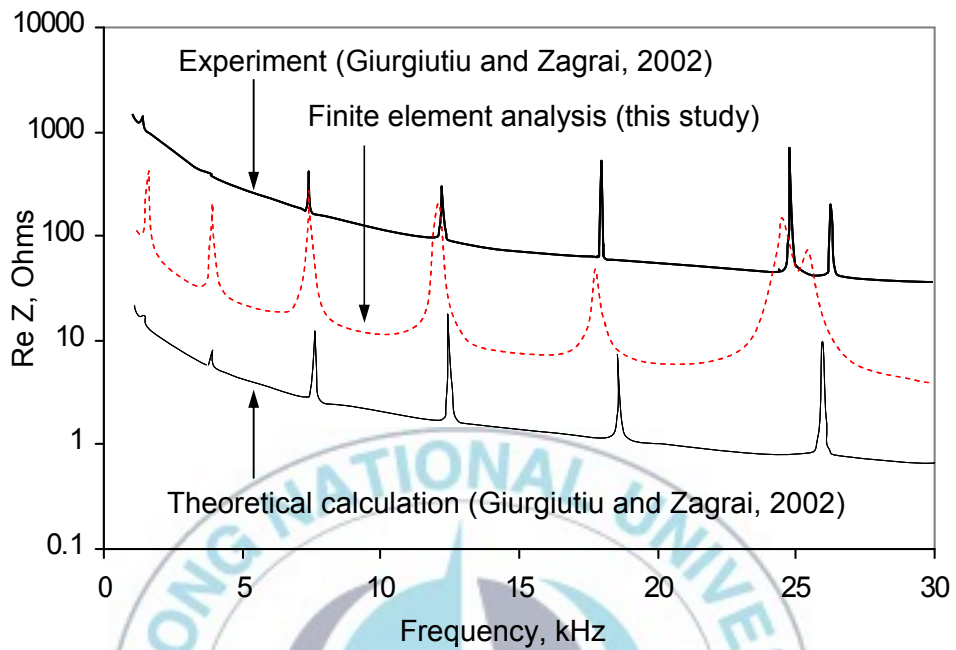


Figure 3.4 Impedance signatures of free-free beam

Table 3.2 Resonance frequencies from experimental, theoretical and FE analysis

Experiment (Giurgiutiu and Zagrai, 2002)	Theoretical calculation (Giurgiutiu and Zagrai, 2002)		FE analysis (This study)	
	Freq. (kHz)	Error (kHz)	Freq. (kHz)	Error (kHz)
1.390	1.396	0.006	1.4	0.01
3.795	3.850	0.055	3.7	-0.095
7.4025	7.547	0.1445	7.3	-0.1025
12.140	12.475	0.335	11.9	-0.24
17.980	18.635	0.655	17.7	-0.28
24.840	-	-	24.6	-0.24
26.317	26.035	-0.282	25.4	-0.917

3.3 EM Impedance Analysis for a Cantilever Beam

As another example, a cantilever beam was selected to verify the performance of FE analysis of EM impedance. Experiment on a steel beam which is clamped at one end is carried out as shown in Fig. 3.5. This beam is longer, wider and thicker than the beam studied by Giurgiutiu and Zagrai (2002). The dimensions of the beam are 380 mm in length, 31.5 mm in width, and 4 mm in thickness. A PZT-5A patch whose size is selected as 20x10x0.5 mm is embedded on the cantilever beam at 200 mm distant from the free end. Geometries of the beam and the PZT patch are described in Fig. 3.6. Material properties of the PZT patch are given in Table 3.1. Material properties of the steel beam are assumed as follows: Young's modulus, $E = 200$ GPa, mass density, $\rho = 7850$ kg/m³, and mechanical loss factor, $\eta = 0.02$. An FE model of the cantilever beam is also established using COMSOL 3.4 software as shown in Fig. 3.7.

EM impedance signatures by experiment and FE analysis are shown in Fig. 3.8. The numerical impedance signature is well matched with the experimental one even though the structure is more complicated than that in Giurgiutiu and Zagrai's study (2002).



Figure 3.5 Experimental setup of cantilever beam

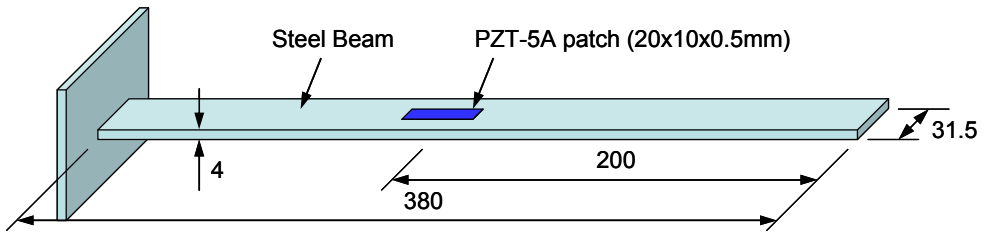


Figure 3.6 Geometry of cantilever beam (Unit: mm)



Figure 3.7 FE model of cantilever beam

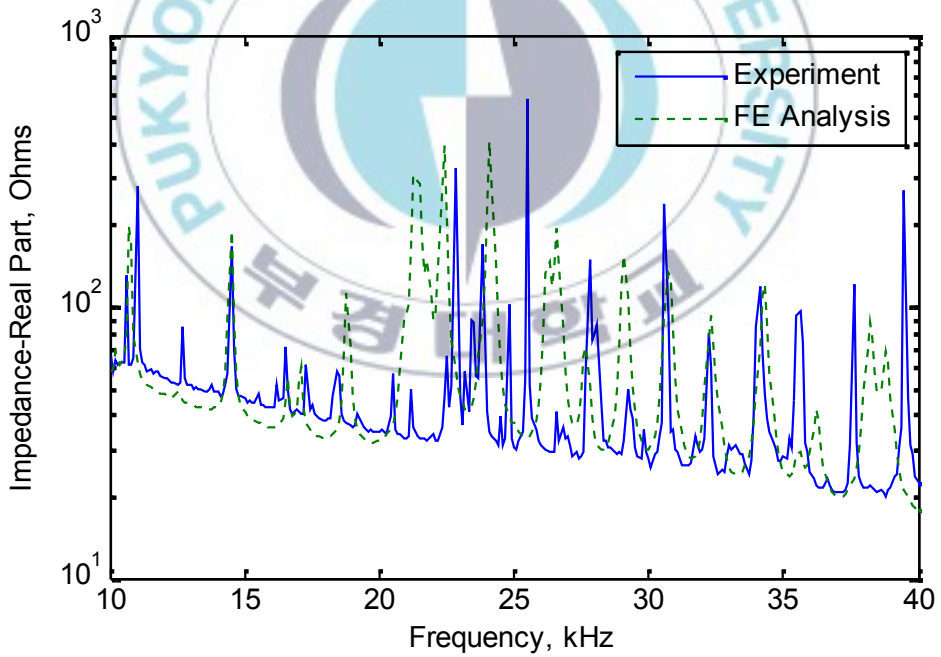


Figure 3.8 Impedance signatures of cantilever beam

CHAPTER 4

INTERFACE WASHER FOR STRUCTURAL CONNECTION MONITORING

4.1 Introduction

In this chapter, a high-sensitive interface washer is designed for structural connection monitoring. Firstly, some issues of impedance-based method in real scale structure are pointed out. Secondly, an interface washer is designed as a way for overcoming the problems.

4.2 Issues of Conventional Impedance-Based Method

Even though the impedance-based method shows the excellent performance in structural health monitoring on many various aspects, this method still has some limitations for civil engineering applications. The drawbacks can be pointed out as follows:

- (1) In order to measure EM impedance, a bulky impedance analyzer is usually used. However, this device is not designed to work out of laboratory. Moreover, the cost associated with the wired system using this device is very high. Efforts to overcome these disadvantages have been carried out by adopting wireless impedance device (Mascarenas et al., 2007; Park et al., 2010a; Park et al., 2010b; Park et al., 2011; Kim et al., 2011). In order to apply the new approach, however, the measurable frequency range of 10 kHz - 100 kHz of the wireless sensors should be dealt appropriately for impedance measurement as well as feature extraction. This frequency range is relatively low compared with that of impedance analyzer. The low frequency may interfere with wide applications in real structures.
- (2) In order to employ the impedance-based method for damage detection, the frequency range which is sensitive to damage has to be identified. Generally, the effective frequency range is various

depending on target structures and usually determined by trial and error. This causes difficulty when applying the impedance-based method to real structure since the effective frequency range is almost unknown and may take much effort to obtain it by trial and error.

The above-mentioned limitations could be overcome by employing an interface washer designed in the next section

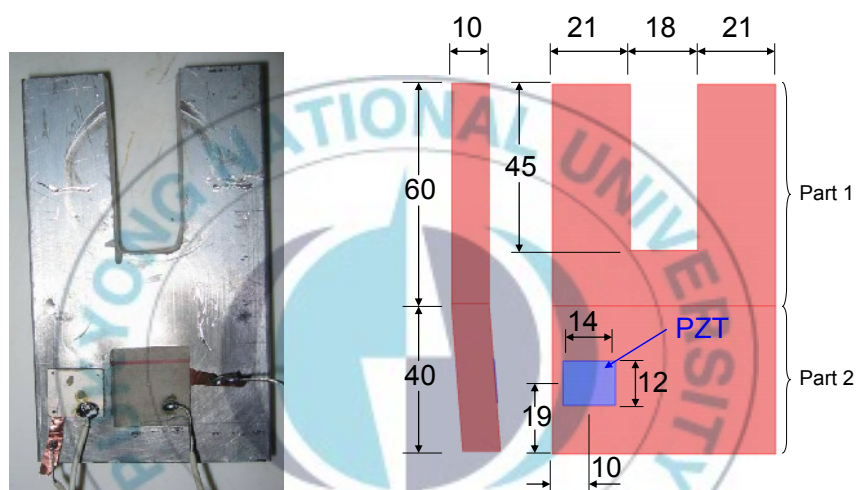
4.3 Interface Washer for Compressive Force Monitoring

One kind of interface washer was utilized for bolt loosened monitoring by Mascarenas et al. (2006). In that study, a tube-shaped washer was installed on a bolt the same way as bolt washer. By increasing bolt preload, mechanical impedance of the system increased, and then the amplitude of EM impedance was damped out. The authors utilized the amplitude level of EM impedance as a damage index. However, the amplitude was damped out so significantly in high preload that the peak might not be observed. In this study, another kind of interface washer which is sensitive to high level of compressive force is designed to represent the loss of preload in structural connection.

4.3.1 Description of Interface Washer

An interface washer equipped with a PZT patch is designed as shown in Fig. 4.1. The interface washer is made of aluminum, and its entire dimension is 100x60x10 mm. The PZT patch is PZT-5A type and its size is selected as 14x12x0.2 mm. Material properties of the PZT patch and the interface washer are given in Table 3.1 and Table 4.1, respectively. Geometries of the interface washer and the PZT patch are described in detail in Fig. 4.1(b). The PZT patch is surface-bonded on the interface washer at 10 mm from the left edge and 19 mm from the bottom edge of the interface washer. Basically, the interface washer can be separated into two parts. Part 1 is installed to structural connection and held by compressive force, and

part 2 is flexible plate which is vibrated by the PZT patch. Figure 4.2 shows how the interface washer can be utilized for monitoring compressive force loss of cable-anchor system. As shown in Fig. 4.2, the interface washer is attached between an anchorage and a steel plate. By this way, any change in anchor force will be represented by the changes in boundary condition and stress field of the interface washer, which in turn affects the EM impedance from the PZT patch.



(a) Interface washer (b) Geometries of interface washer and PZT patch (Unit: mm)

Figure 4.1 Interface washer for compressive force monitoring

Table 4.1 Material properties of interface washer

Quantity	Value
Young's modulus, E (GPa)	70
Poisson's ratio, ν	0.33
Mass density, ρ (kg/m^3)	2700
Damping loss factor, η	0.02

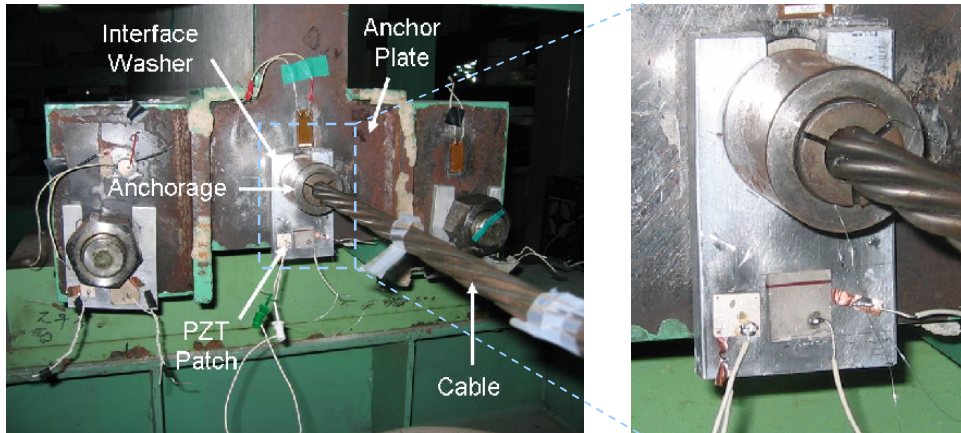


Figure 4.2 Installed interface washer in cable-anchor connection

4.3.2 Advantages of Interface Washer

The advantages of interface washer are as follows: (1) the effective frequency range of impedance is known; and (2) it can be controlled by designing the specifications of the interface washer as well as the PZT patch. Therefore, it can be installed to many different connection types. Another benefit of using interface washer is that the effective frequency range of impedance is relatively low, that is measurable by wireless impedance devices. To evaluate the performance of the interface washer on compressive force monitoring in low frequency range, two FE models of cable anchor connection without and with interface washer (model A and model B) are established as shown in Figs. 4.3 and 4.4, respectively.

In model A (Fig. 4.3), a PZT patch is directly bonded on the anchor plate to monitor the change in anchor force. For boundary condition of the anchor plate, the backward surface which does not contain the PZT patch is fixed, and the remaining surfaces are freely deformed. Anchor force is applied at the middle-centre of the anchor plate as shown in Fig. 4.3. In model B (Fig. 4.4), the anchor force is monitored by the PZT patch attached on the interface washer. To examine the change in the EM impedance signatures due to the change in anchor force, two force levels are applied as 79.5 kN and 72.6 kN to each model.

EM impedance signatures of two models A and B are shown in Figs. 4.5 and 4.6, respectively. As shown in Fig. 4.5, there is no peak obtained for model A and the differences in impedance signatures for two force levels can not be observed. On the other hand, some feasible peaks are obtained in impedance signatures for model B as shown in Fig. 4.6. Also, the change in impedance signatures due to the change in anchor force can be observed. It is worth noting that the impedance signature is more sensitive to structural change at resonance. In order to quantify the performances of two models A and B to anchor force, a comparison of RMSD indices of impedance signatures for the two models is performed in Fig. 4.7. It is found that the value of RMSD for model A is very small compared with that for model B. This indicates that the impedance signature from the PZT patch on the anchor plate is less sensitive to change in compressive anchor force.

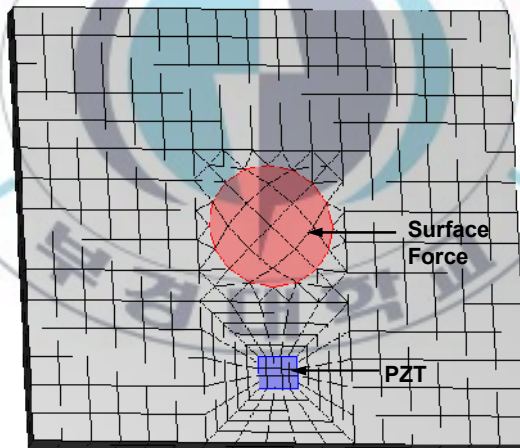


Figure 4.3 FE model of cable anchor connection without interface washer (model A)

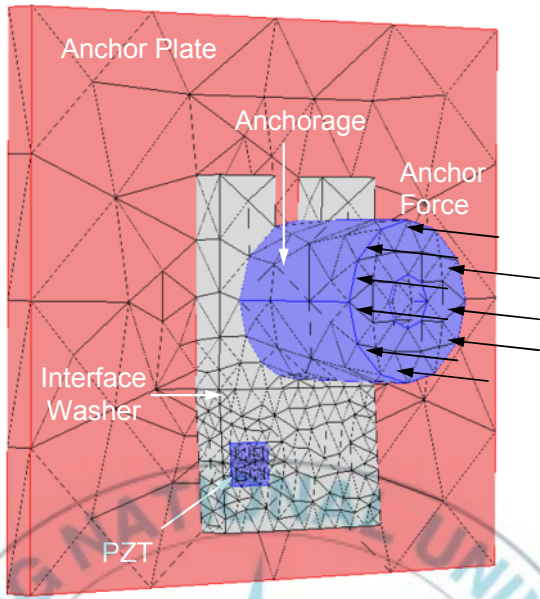


Figure 4.4 FE model of cable-anchor connection with interface washer (model B)

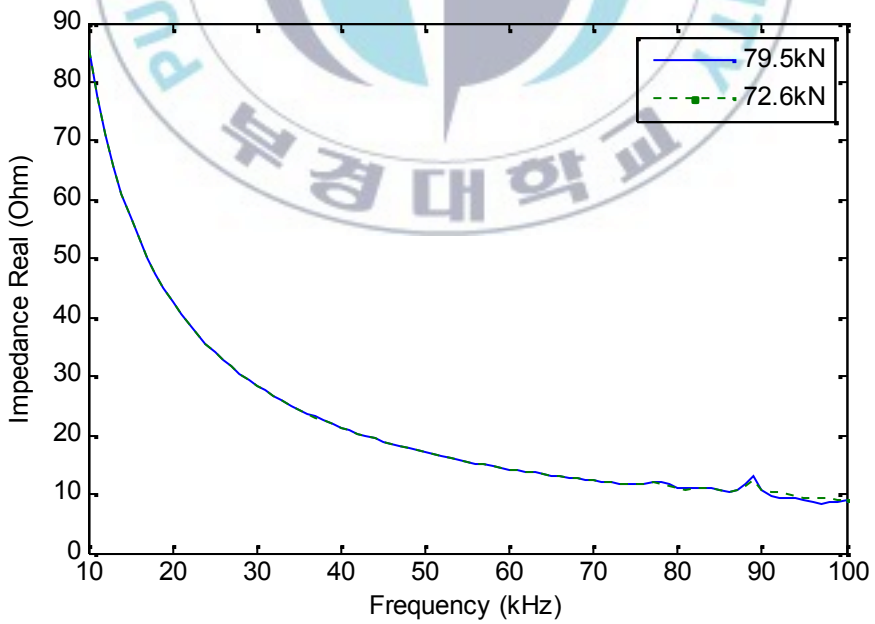


Figure 4.5 Impedance signatures for model A

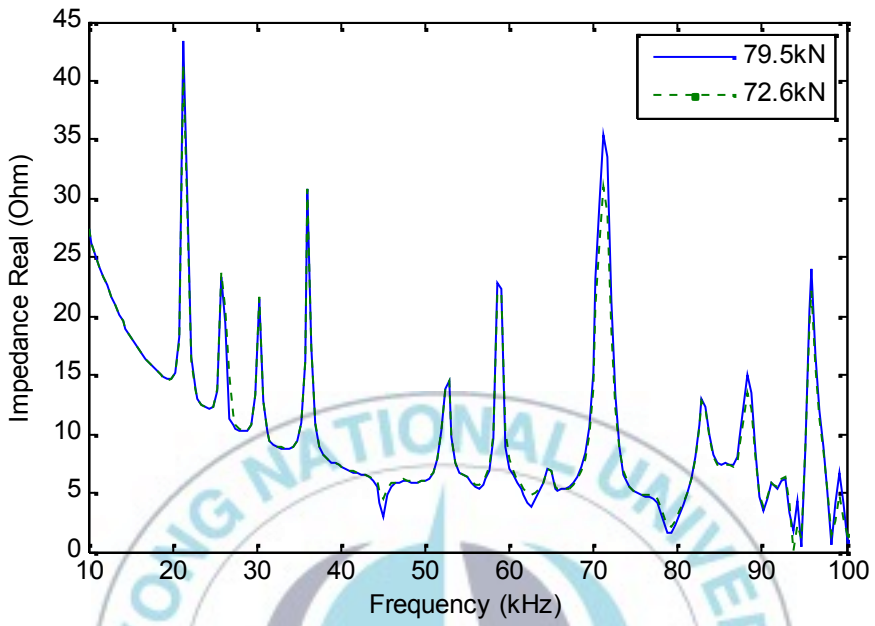


Figure 4.6 Impedance signatures for model B

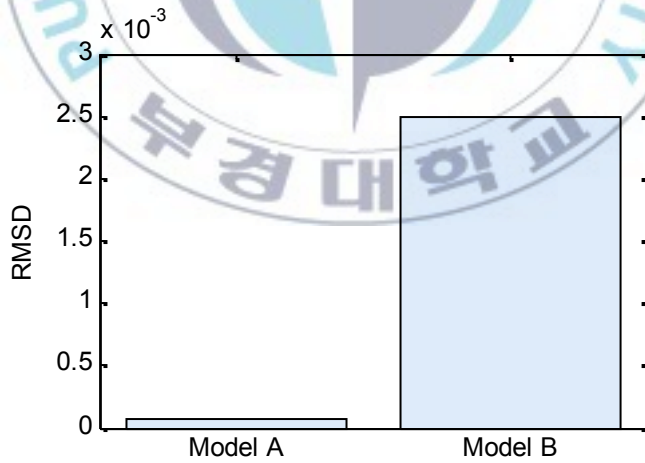


Figure 4.7 RMSD indices for two models A and B

CHAPTER 5

FE ANALYSIS OF EM IMPEDANCE FOR CABLE ANCHOR CONNECTION

5.1 Introduction

In this chapter, FE analysis of EM impedance is performed for a cable-anchor connection. Firstly, an FE model of cable-anchor connection with an installed interface washer is established. Secondly, the approach of static-dynamic coupled impedance analysis is described to examine the effect of anchor force on EM impedance responses. Thirdly, the FE analysis is verified by experiment on a lab-scale cable-anchor connection. Finally, the effects of material and geometrical properties of interface washer on EM impedance are investigated.

5.2 FE Analysis of EM Impedance for Cable-Anchor Connection

5.2.1 Description of FE Model

To evaluate the performance of the interface washer on anchor force loss monitoring, an FE model of cable-anchor connection is established. The purposes of this simulation are to examine the patterns of EM impedance signature due to the loss of anchor force and so far to establish baseline model of cable-anchor connection. Figure 5.1 shows experimental setup of a cable-anchor connection. As shown in Fig. 5.1, an interface washer is installed between an anchor plate and an anchorage. The interface washer is held on the connection by compressive anchor force caused by tensioning the cable. The interface washer in this situation works like a cantilever plate.

In order to select the suitable frequency range for anchor force monitoring, two experiments correspondent to two anchor forces as 79.5 kN and 72.6 kN are carried out. The cable-anchor connection under the two forces is in undamaged and damaged condition, respectively. For each anchor force, EM impedance is measured in various frequency ranges from 10 kHz to 100 kHz. Figures 5.2, 5.3, and 5.4 show the impedance signatures

in typical frequency ranges as 30 kHz - 40 kHz, 60 kHz – 70 kHz, and 10 kHz – 100 kHz, respectively. RMSD indices of the impedance signatures for damaged case (anchor force loss) are then calculated at ten frequency ranges as shown in Fig. 5.5. The RMSD for the wide frequency range of 10 kHz – 100 kHz is relatively high compared with that for the narrow frequency ranges of 10 kHz interval. That means using the wide frequency range is feasible for anchor force monitoring. However, for the higher sensitivity, the narrower frequency range of 30 kHz – 40 kHz or 60 kHz – 70 kHz should be selected. In this study, the impedance signatures in frequency range of 30 kHz – 40 kHz is examined since the impedance signatures in this range is highly sensitive to anchor force change.

According to the experimental setup, an FE model of cable-anchor connection is established as shown in Fig. 5.6. The FE model includes an anchor plate, an interface washer equipped with a PZT patch, and an anchorage. The anchor plate and the anchorage are both made of steel with material properties are summarized in Table 5.1. Viscous damping is assumed for the FE model with damping loss factor (η) as 0.02 for the anchor plate, the anchorage, the interface washer; and 0.0125 for the PZT patch. Material properties of the PZT patch and the interface washer are given in Table 3.1 and Table 4.1, respectively.

To include the effect of anchor force on EM impedance, the distributed static force is simulated on flat surface of the anchorage as shown in Fig. 5.6. The change in anchor force would result the changes in structure's dynamic responses, which are expected to be represented by changes in EM impedance. To examine the effect of anchor force on EM impedance response, four FE models of cable-anchor connection correspondent to four levels of anchor force as 79.5 kN, 72.6 kN, 66.7 kN and 60.8 kN are established.

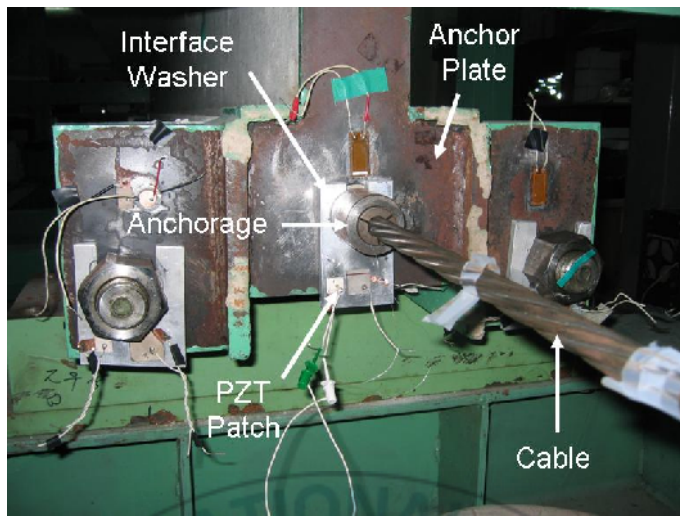


Figure 5.1 Experimental setup of cable-anchor connection

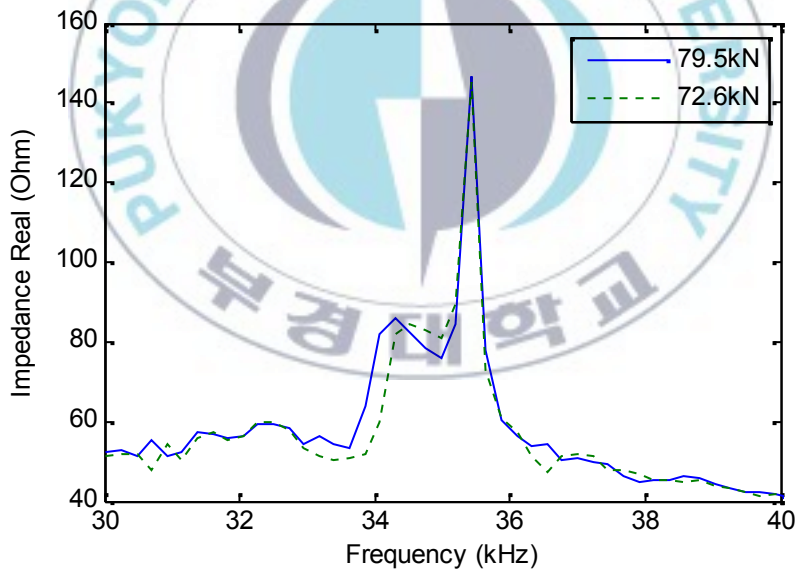


Figure 5.2 Experimental impedance signatures in frequency range of 30 kHz – 40 kHz

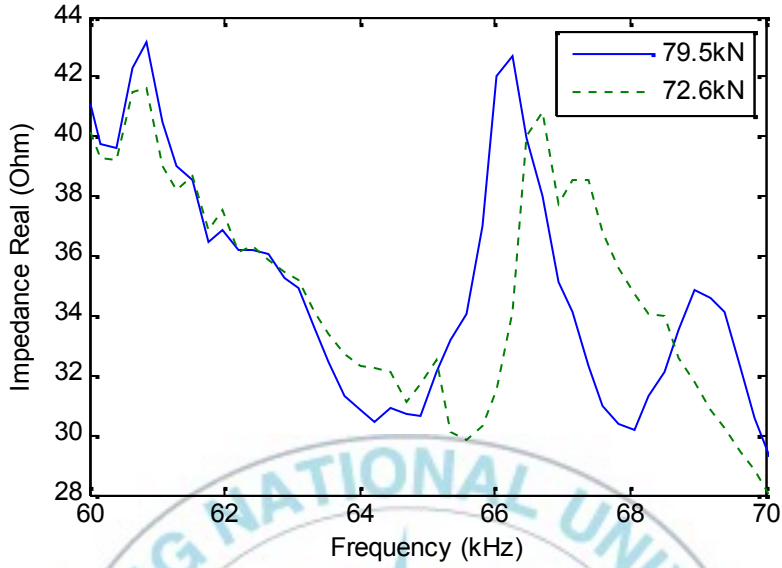


Figure 5.3 Experimental impedance signatures in frequency range of 60 kHz – 70 kHz

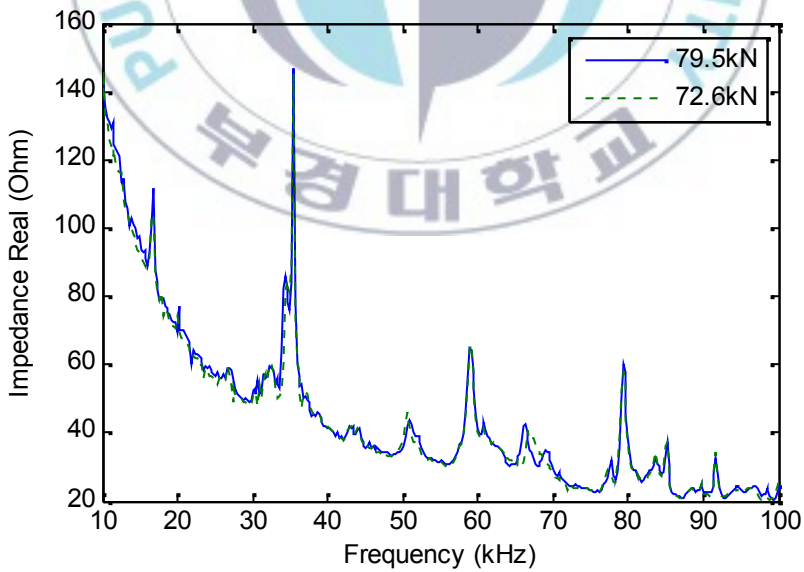


Figure 5.4 Experimental impedance signatures in frequency range of 10 kHz – 100 kHz

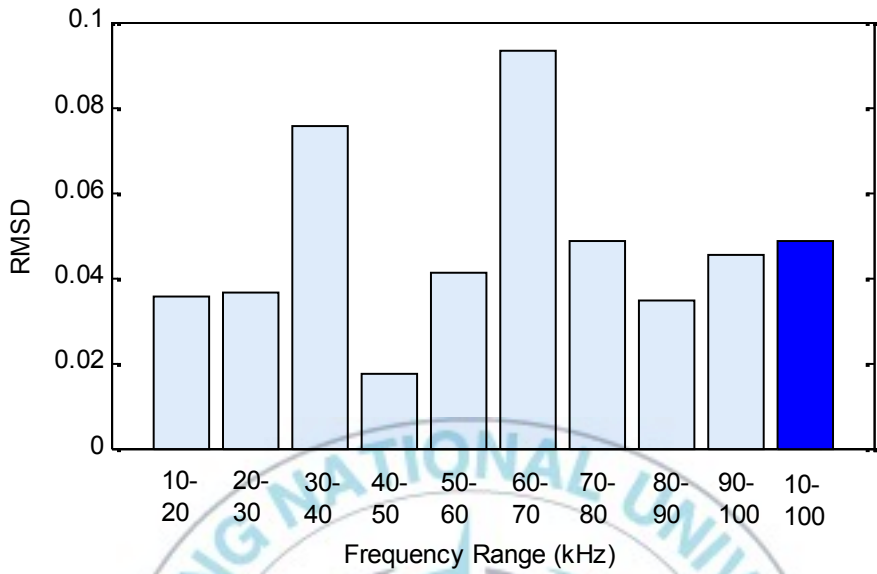
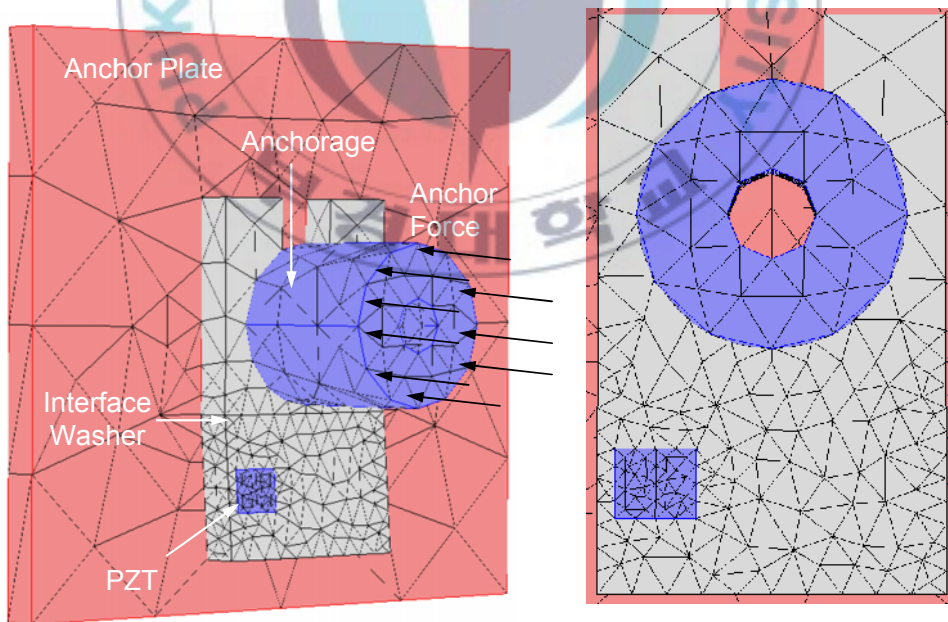


Figure 5.5 RMSD indices for various frequency ranges (Experiment)



(a) Cable-anchor connection

(b) Top view at interface washer

Figure 5.6 FE model of cable-anchor connection

Table 5.1 Material properties of anchor plate and anchorage

Quantity	Value
Young's modulus, E (GPa)	200
Poisson's ratio, ν	0.3
Mass density, ρ (kg/m ³)	7850
Damping loss factor, η	0.02

5.2.2 Static-Dynamic Coupled Impedance Analysis

For the cable-anchor connection, anchor force affects statically to the connection while excitation voltage produces dynamic behavior on the connection. Therefore, a static-dynamic coupled impedance analysis must be performed to obtain the EM impedance of cable-anchor connection. The procedure of static-dynamic coupled analysis of EM impedance is summarized in Fig. 5.7. For convenience, the FE model with structural geometry, material properties and boundary condition is named as model A. For each level of anchor force, model A is first run with only static anchor force (without harmonic voltage) to obtain initial values (i.e., stresses, strains, and displacements), and geometry stiffness caused by anchor force. The solutions of the static analysis is then stored for using in next step. After that, model A with including the solutions stored in the static analysis is dynamically analyzed with excitation voltage. A harmonic voltage of 2 V is applied to the upper surface of the PZT patch while the lower surface is electrical ground. By the static-dynamic coupled analysis, effects of both anchor force and harmonic voltage are included in the model.

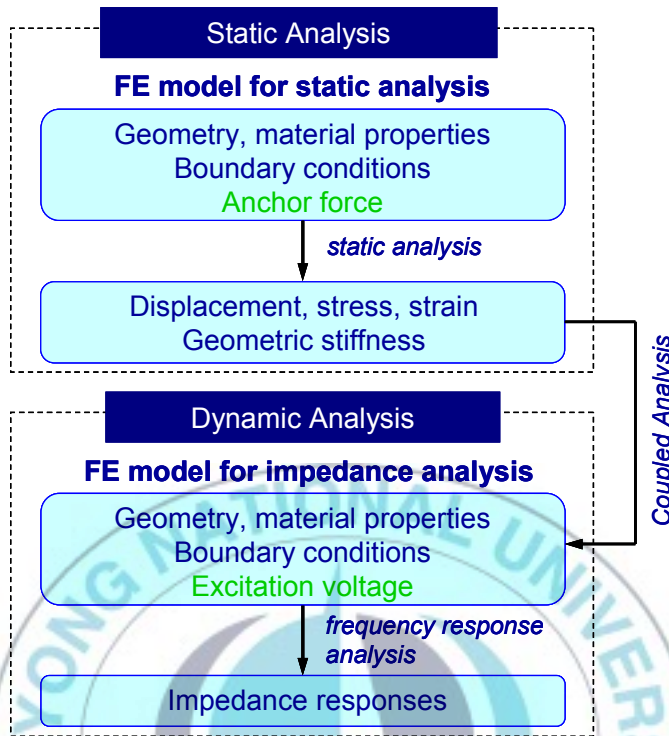


Figure 5.7 Static-dynamic coupled impedance analysis

5.2.3 Effect of Anchor Force on EM Impedance Signature

After the static-dynamic coupled impedance analysis process was completely run, impedance responses of the cable-anchor connection were obtained. Figure 5.8 shows deformations of the cable-anchor connection at 36.16 kHz due to various levels of anchor force. As shown in Fig. 5.8, the deformation of anchorage becomes smaller since anchor force decrease (the color becomes darker). EM impedance signatures of the cable-anchor system are then calculated for various anchor forces. Since most of mechanical impedance of structure is presented in real part of EM impedance signature, only the changes in real part of EM impedance signature are monitored. Figure 5.9(a) shows EM impedance signatures (real part) in frequency range from 30 kHz to 40 kHz for various anchor forces. As shown in the figure, the impedance signatures obtained by FE analysis

are resonant around 36.16 kHz. The closer looking at impedance signatures in frequency range of 36.1 kHz - 36.2 kHz with interval of 10 Hz is performed in Fig. 5.9(b). By examining impedance resonance, the amplitude of resonance is reduced due to the loss of anchor force as shown in Fig. 5.10. Meanwhile, the resonance frequency remains unchanged since anchor force decreases.

In order to examine the effect of anchor force loss on EM impedance in the whole frequency range, root mean square deviation (RMSD) index, mean absolute percentage deviation (MAPD) index and correlation coefficient deviation (CCD) index which are described in Eqs. (2.6), (2.7), (2.8), respectively, are calculated. RMSD, MAPD and CCD indices due to the loss of anchor force are given in Fig. 5.11. As shown in the figure, by FE analysis, the CCD is not changed since anchor force increases. Meanwhile, the RMSD and the MAPD both tend to increase since anchor force increases. However, the RMSD is more sensitive to change in anchor force. Therefore, by using RMSD as a damage index, all cases of anchor force loss can be indicated.

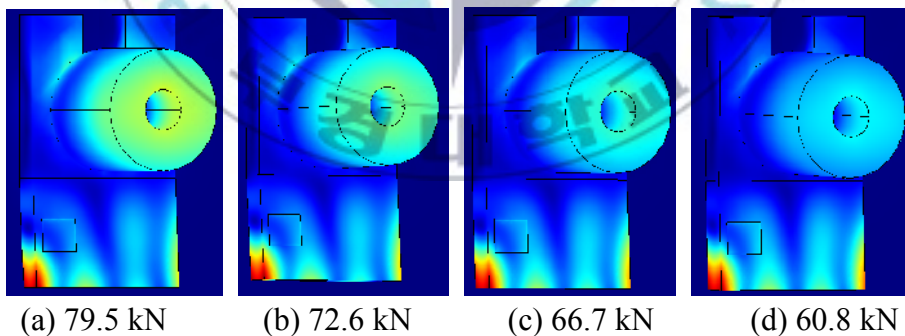
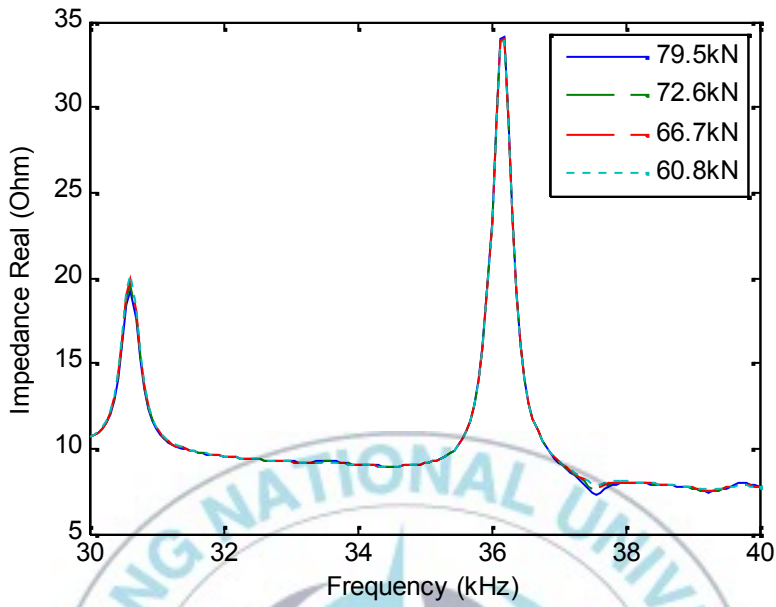
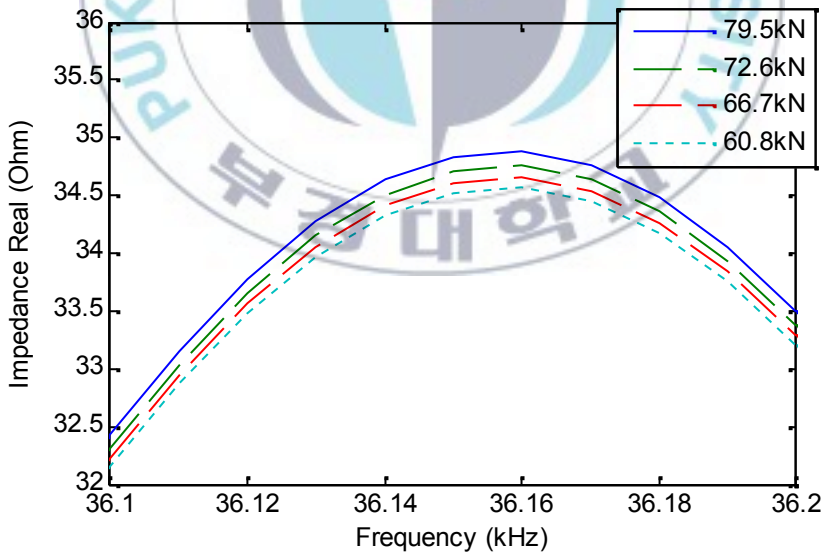


Figure 5.8 Deformations of cable-anchor connection at 36.16 kHz



(a) Frequency range: 30 kHz - 40 kHz



(b) Frequency range: 36.1 kHz - 36.2 kHz

Figure 5.9 Numerical impedance signatures for various anchor forces

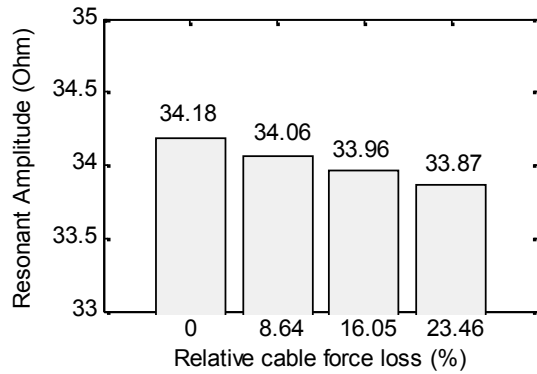
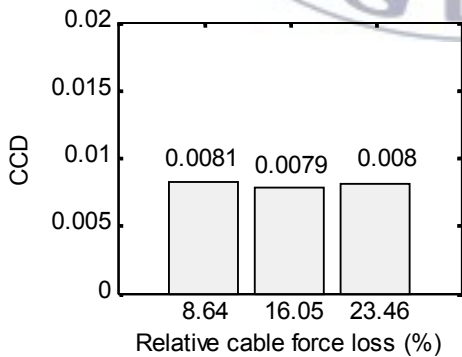
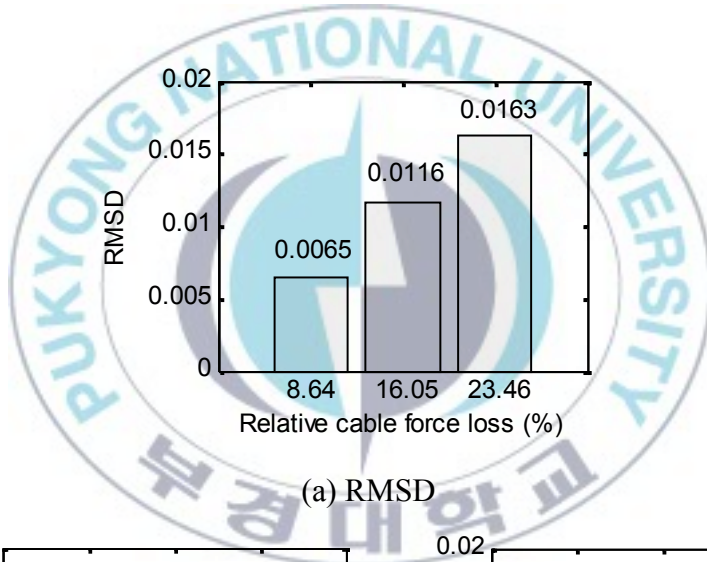
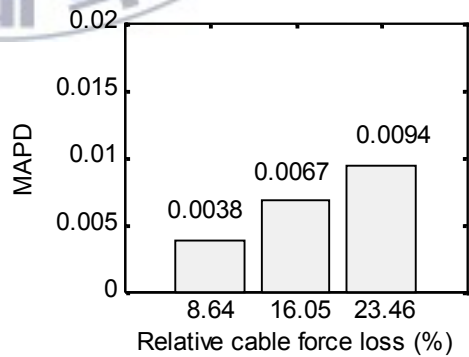


Figure 5.10 Impedance real values at 36.16 kHz (FE analysis)



(b) CCD



(c) MAPD

Figure 5.11 Statistical damage indices due to loss of anchor force (FE analysis)

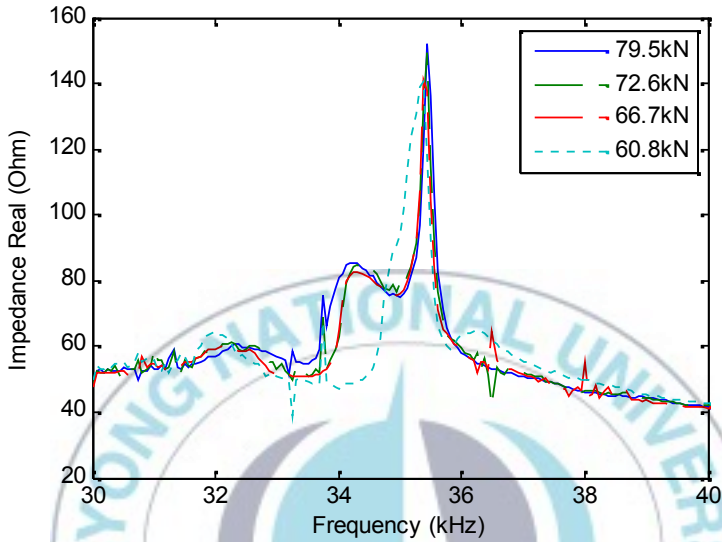
5.3 Experimental Verification for Cable-Anchor Connection

To verify the feasibility of the FE analysis, experiment on a lab-scale cable-anchor connection was carried out as shown in Fig. 5.1. In the experiment, four levels of anchor force (79.5 kN, 72.6 kN, 66.7 kN and 60.8 kN) which are the same as those in the FE analysis were sequentially applied to the anchorage. Among them, the connection with anchor force of 79.5 kN was considered as the healthy state, and the others were in damaged conditions. A wireless impedance sensor node (Park et al., 2010a) was used to excite the PZT patch and measure EM impedance. The PZT patch was excited with a harmonic voltage of 2 V in frequency range of 30 kHz - 40 kHz. Figure 5.12(a) shows EM impedance signatures from 30 kHz to 40 kHz for the cable-anchor connection under four levels of anchor force. Resonance frequency is found around 35.5 kHz which is quite close to the numerical one (36.16 kHz). In order to investigate the change in EM impedance at resonance, the impedance signatures in frequency range of 35.3 kHz - 35.6 kHz are performed in Fig. 5.12(b). As shown in the figure, impedance amplitude at resonance decreases since anchor force decreases. Such pattern is successfully reflected by the FE analysis. The amplitudes of resonance impedance are shown in detail in Fig. 5.13(a).

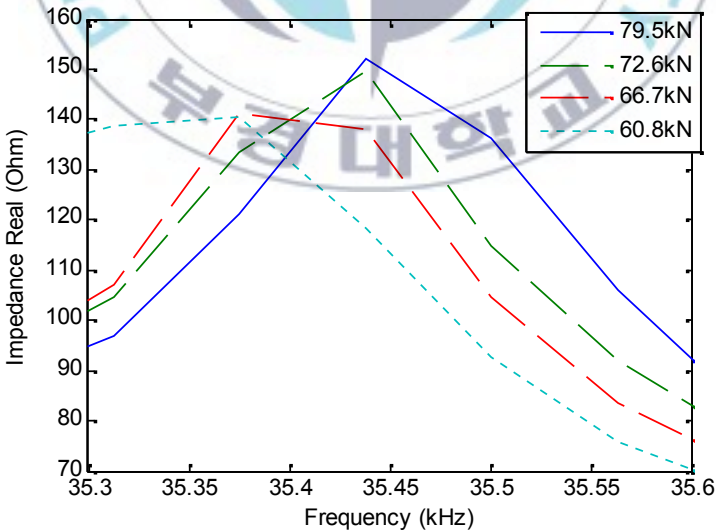
The shift of resonance frequency due to the loss of anchor force is also investigated as shown in Fig. 5.13(b). It is found that, since anchor force decreases the peak of impedance signature tends to shift to lower frequency. On the contrary, the frequency shift is not observed by the FE analysis. This could be explained by that, the interaction between the interface washer and the anchor plate as well as between the interface washer and the anchorage may become weaker when anchor force decreases. Meanwhile, in the FE model, this interaction is assumed unchanged since the strength reduction in this kind of interaction could not be simulated.

For examination of EM impedance signatures in the whole frequency range, RMSD, MAPD, and CCD indices of EM impedance signatures are once more employed. Figure 5.14 shows these indices due to the loss of

anchor force. As shown in the figure, all the statistical indices increase since anchor force is reduced. Such pattern is also successfully reflected by the FE analysis except for the CCD index.

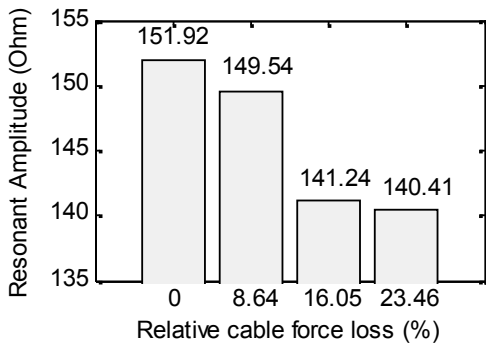


(a) Frequency range: 30 kHz - 40 kHz

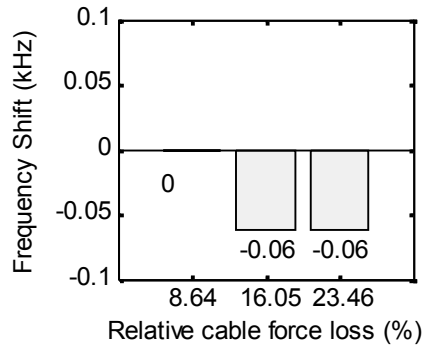


(b) Frequency range: 35.3 kHz - 35.6 kHz

Figure 5.12 Experimental impedance signatures for various anchor forces

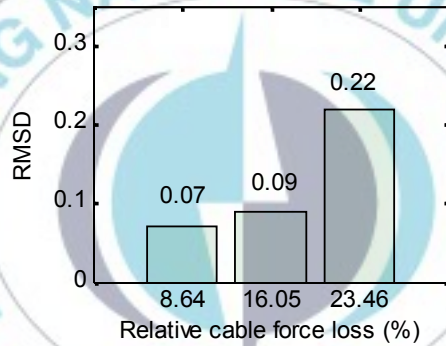


(a) Resonance impedances

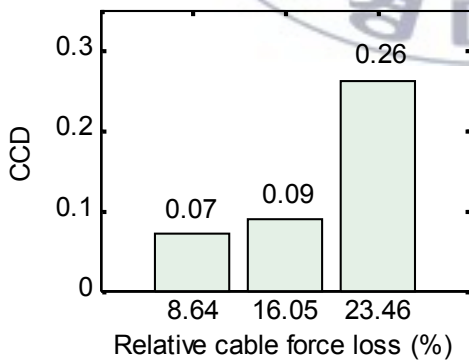


(b) Frequency shift

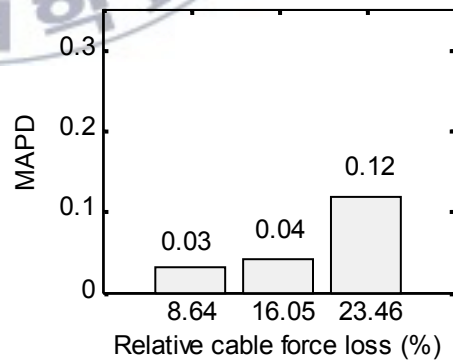
Figure 5.13 Resonance impedance and frequency shift results (Experiment)



(a) RMSD



(b) CCD



(c) MAPD

Figure 5.14 Statistical damage indices due to loss of anchor force (Experiment)

5.4 Design of Interface Washer

5.4.1 Effect of Material Properties of Interface Washer on EM Impedance Signature

In the FE model above, the interface washer made of aluminum was designed to monitor the cable-anchor connection. The effect of material properties of interface washer on EM impedance responses is investigated by modeling a cable-anchor connection equipped with a steel interface washer. Simplicity, material properties of the interface washer are changed as follows: Young's modulus, $E = 200$ GPa; Poisson's ratio, $\nu = 0.33$; mass density, $\rho = 7850$ kg/m³. Damping loss factor of the steel interface washer is kept as same as that of the aluminum one.

EM impedance signatures of the cable anchor connection under four levels of anchor force are then calculated as shown in Fig. 5.15. Resonance frequencies of the impedance signatures by using the steel interface washer are around 35.69 kHz which is slightly shifted left (or decreased) compared with those by using the aluminum one (36.16 kHz). That shifting could be explained by considering ratios of Young's modulus to mass density for two kinds of material. The ratio for steel is 0.0255 which is slightly smaller than that for aluminum, 0.0259. As a result, the resonance frequencies of impedance signatures by using the steel interface washer are smaller.

By analyzing the impedance amplitude at resonance due to the loss of anchor force, the same pattern as using the aluminum interface washer is obtained. The impedance amplitude at resonance is reduced due to the loss of anchor force. RMSD indices according to the loss of anchor force are analyzed to evaluate the sensitivity of the steel interface washer. Figure 5.16 shows the comparison of RMSD indices when using the aluminum interface washer and the steel one. As shown in the figure, the RMSD indices when using the steel interface washer are increased since anchor force reduces. The RMSD indices by using steel interface washer are lightly lower than those by using aluminum one. Note that, the elastic modulus and the mass density of steel is much larger than those of aluminum (about 3 times for

each parameter). Therefore, Young's modulus and mass density of interface washer material contribute insignificant effect on sensitivity of interface washer to impedance signature. It is also worth noting that, damping loss factor of the steel interface washer was assumed as same as that of the aluminum one since it needs much effort to obtain the exact value of damping. This parameter may affect the sensitivity of EM impedance signature to anchor force loss. This issue will be examined in future study.

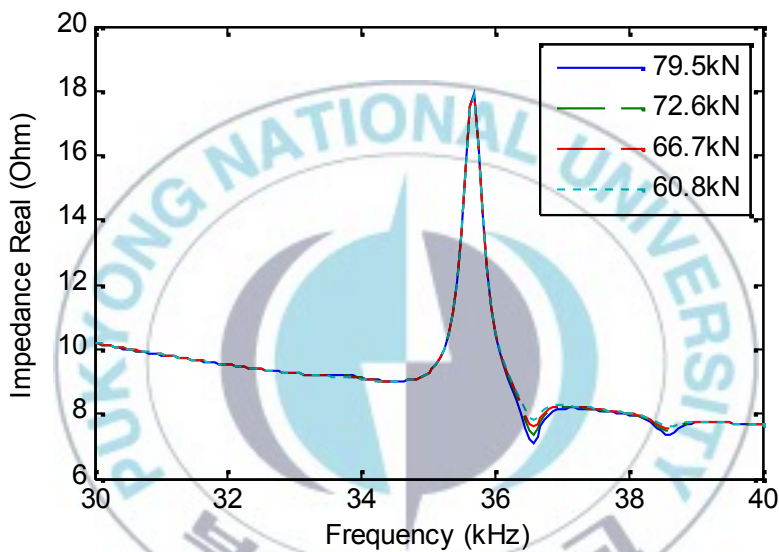


Figure 5.15 Numerical impedance signatures of cable anchor connection with steel interface washer

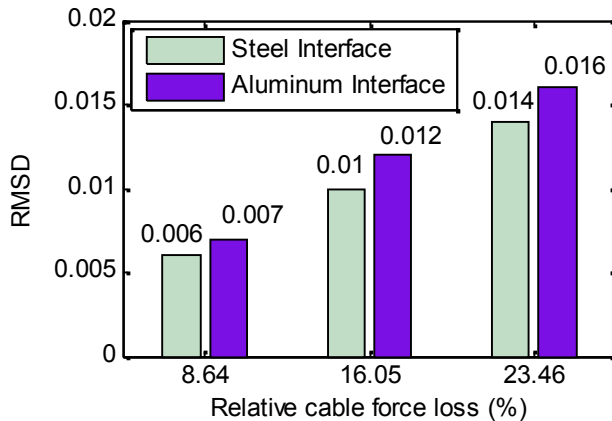


Figure 5.16 RMSD indices by using aluminum and steel interface washers (FE analysis)

5.4.2 Effect of Geometrical Properties of Interface Washer on EM Impedance Signature

To analyze the effect of geometrical properties of interface washer on EM impedance signature, four interface washers with different thicknesses, 0.6 cm, 0.8 cm, 1.0 cm, and 1.2 cm, are modeled in cable-anchor connection. Material of the interface washers is aluminum. For each kind of interface washer, FE models of cable-anchor connection correspondent to two levels of anchor force (79.5 kN and 72.6 kN) are established. The model with 79.5 kN is considered as the healthy connection, the latter is in damaged condition with 8.64% loss of anchor force. EM impedance signatures for the interface washers with various thicknesses under 79.5 kN of anchor force are shown in Fig. 5.17. It is found that the impedance peak is damped to lower amplitude and shifted to higher frequency when thickness of the interface washer increases. The decrement of impedance amplitude at resonance may result the decrease of sensitivity of impedance signature to anchor force change.

To analyze the effect of interface washer thickness on sensitivity of impedance signature in the whole frequency range, RMSD index of EM impedance signature is computed when anchor force is lost. As mentioned

above, the resonance frequency shifts left and right when using the thinner interface washers and the thicker interface washers, respectively. Therefore, the frequency range for investigating is widened from 25 kHz to 50 kHz. Figure 5.18 shows RMSD indices for various thicknesses of interface washer at 8.64% loss of anchor force. It is observed that the RMSD index tends to decrease due to the increment of thickness of the interface washer. This implies that the sensitivity of impedance signature to anchor force loss is reduced when the interface washer becomes thicker. This decrement can be explained by that the interface washer becomes harder to be vibrated by the PZT patch when its thickness increases. It is worth noting that, by using low sensitive interface washer in real-scale structure, the changes in EM impedance signature due to anchor force loss and due to noise might not be separated. Therefore, using interface washer with thickness as small as 0.6 cm can give better results for cable-anchor connection monitoring.

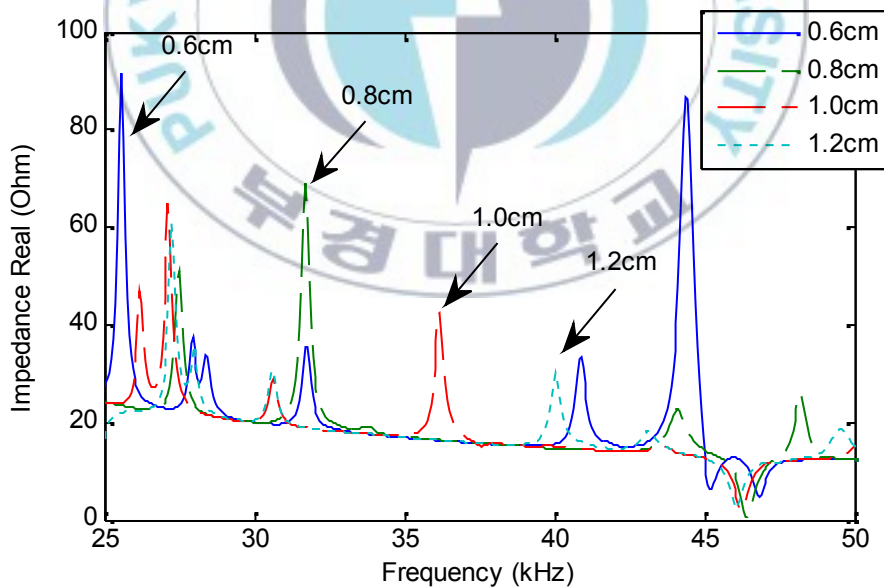


Figure 5.17 Numerical impedance signatures for various thicknesses of interface washer under anchor force of 79.5 kN

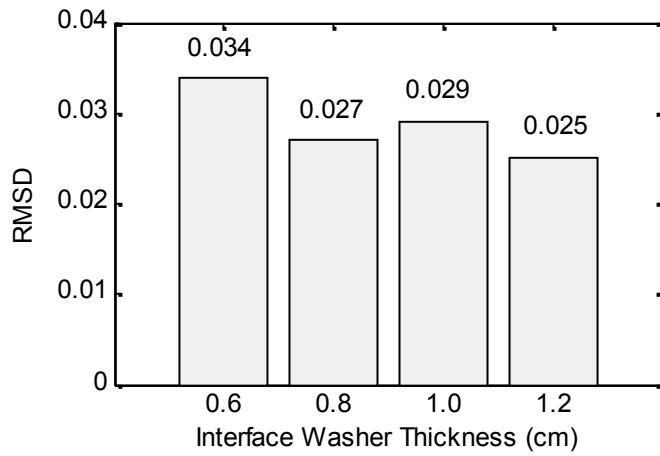
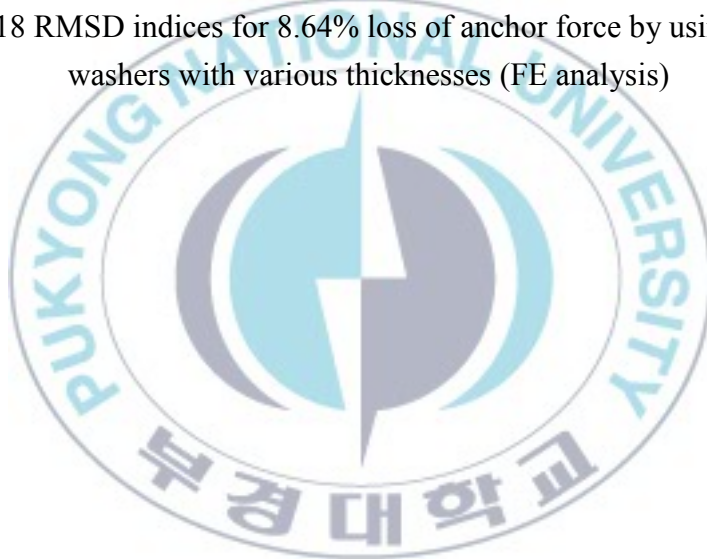


Figure 5.18 RMSD indices for 8.64% loss of anchor force by using interface washers with various thicknesses (FE analysis)



CHAPTER 6

FE ANALYSIS OF EM IMPEDANCE FOR BOLTED CONNECTION

6.1 Introduction

In this chapter, EM impedance of a bolted connection is simulated by FE analysis for bolt loosened monitoring. Firstly, an FE model of bolted connection with an installed interface washer is established. Secondly, EM impedance from the PZT patch is investigated for several cases of bolt loosening. Thirdly, the FE analysis is verified by experiment on a lab-scale bolted connection.

6.2 FE Analysis of EM Impedance for Bolted Connection:

6.2.1 Description of FE Model:

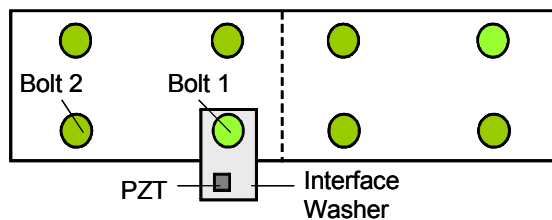
Another example to examine the effect of compressive force on EM impedance is bolted connection. Figure 6.1 shows experimental setup of a bolted connection. The bolted connection consists of 16 bolts which are fastened up to connect two single H-shaped girders at their flanges. An interface washer is installed at one of the bolts (i.e., Bolt 1 in Fig. 6.1 (b)). An FE model of one part of bolted connection is established as shown in Fig. 6.2. According to limitation of computing capability, the FE model is established to cover a small part of the bolted connection, at bottom-left of the connection, around the interface washer. Material properties of the PZT patch and the interface washer are given in Table 3.1 and Table 4.1, respectively. Meanwhile, material properties of the steel plate is assumed as same as those of anchor plate as given in Table 5.1. In the FE model, bolt pressure is simulated by distributed static axial force on the surface of bolt washer. Value of axial force is estimated from bolt torque based on the following equation:

$$N = T/(k.d) \quad (6.1)$$

where N is the equivalent axial force on bolt washer, T is the bolt torque, d is the nominal bolt diameter, and k is the torque coefficient. Considering the bolts are plain non-plated typed, k is assumed as 0.2. The nominal bolt diameter is measured as 2 cm. As the healthy condition, all bolts are fastened to 160 N.m which is equivalent to 40 kN of axial force. The first damage is simulated by loosening Bolt 1 to 35 N.m which is equivalent to 8.75 kN of axial force. The second damage is simulated by loosening Bolt 2 to 35 N.m while Bolt 1 is kept in healthy state. The damage scenarios are summarized in Table 6.1.



(a) Bolted connection



(b) Schematic of bolted connection at one splice

Figure 6.1 Experimental setup of bolted connection

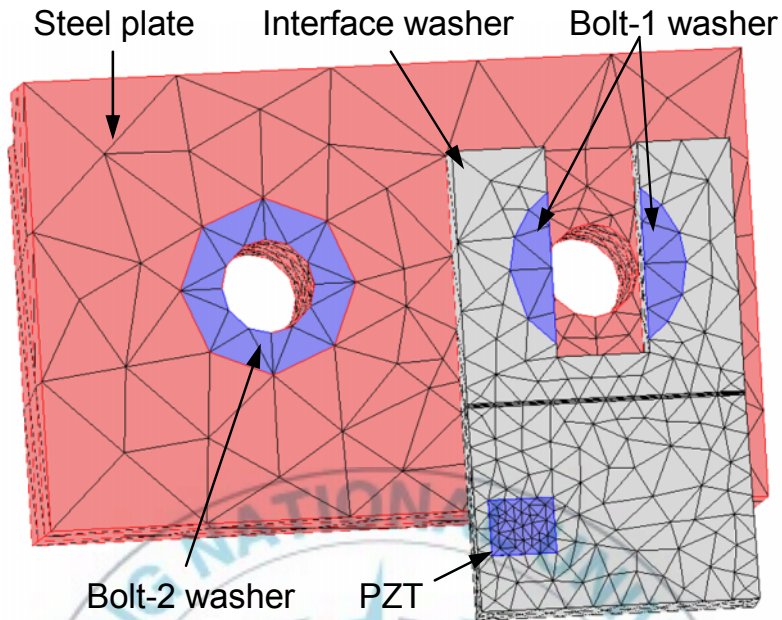


Figure 6.2 FE model of bolted connection

Table 6.1 Bolt loosening scenarios

Model	Description	Equivalent axial force (kN)	
		Bolt 1	Bolt 2
M1	All bolts fastened to 160 N.m	40	40
M2	Bolt 1 loosened by 35 N.m	8.75	40
M3	Bolt 2 loosened by 35 N.m	40	8.75

6.2.2 Effect of Bolt Loosening on EM Impedance Signature

Figure 6.3 shows deformations of three FE models of bolted connection (Table 6.1) at 36 kHz. As shown in the figure, the deformations of models M1 and M3 are almost the same since the deformation of the steel plate around Bolt 2 is very small due to its high elastic modulus. Meanwhile, by loosening Bolt 1, the deformation of the interface washer around Bolt 1 is almost disappeared. EM impedance signatures of model M1, M2 and M3 are compared each other in Figs. 6.4 and 6.5. As shown in Fig. 6.4, the

impedance signature by loosening Bolt 1 is slightly different from that of healthy connection. On the contrary, the impedance signature is almost not changed when loosening Bolt 2 (see Fig 6.5). To examine the effect of the two damages cases on EM impedance signatures, RMSD indices of the impedance signatures for two damage cases are compared each other in Fig. 6.6. The RMSD index when loosening Bolt 2 is very small compared with that when loosening Bolt 1. As a result, the interface washer is feasible for self-monitoring since the loosening of neighbor bolt almost does not affect the EM impedance signature of the connection.

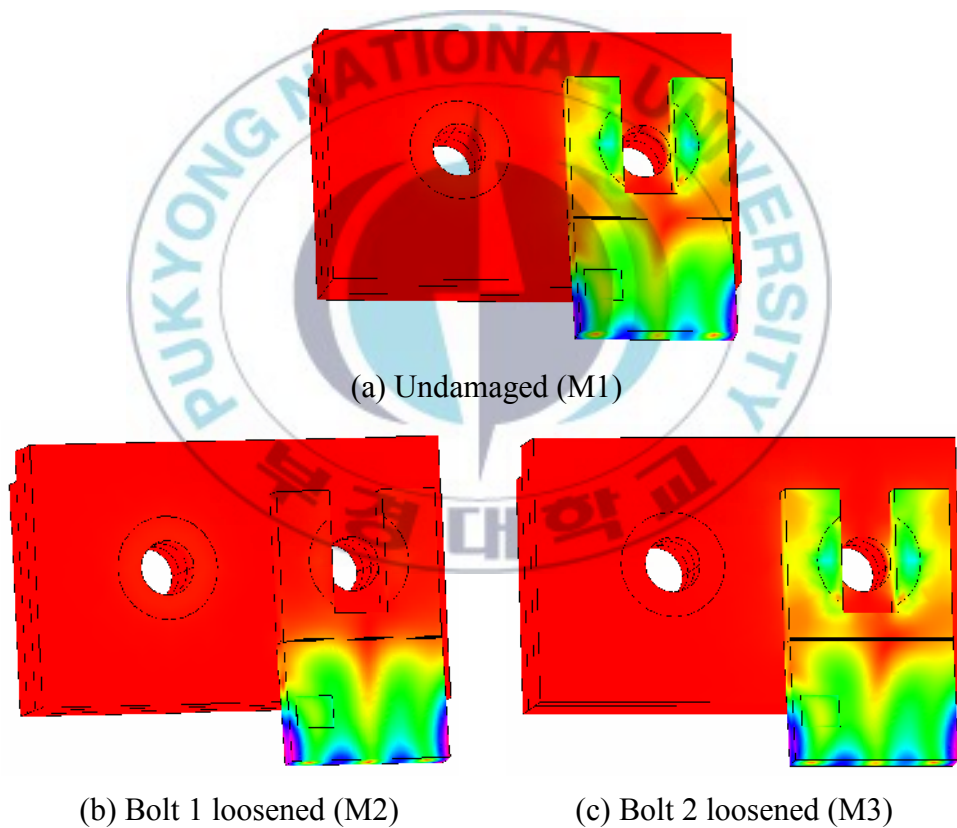


Figure 6.3 Deformations of bolted connection at 36 kHz

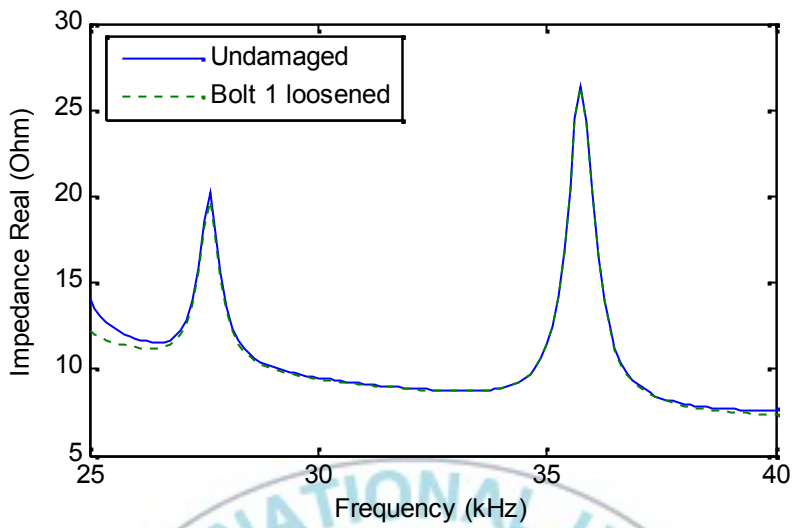


Figure 6.4 Numerical impedance signatures for models M1 and M2

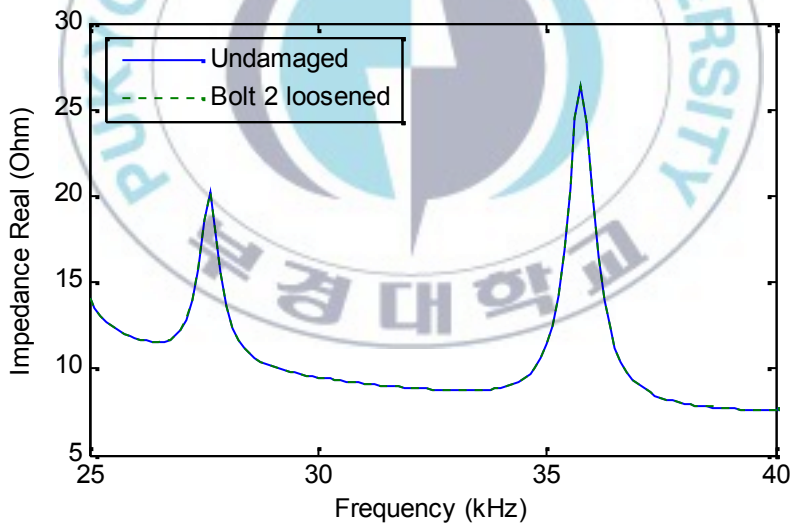


Figure 6.5 Numerical impedance signatures for models M1 and M3

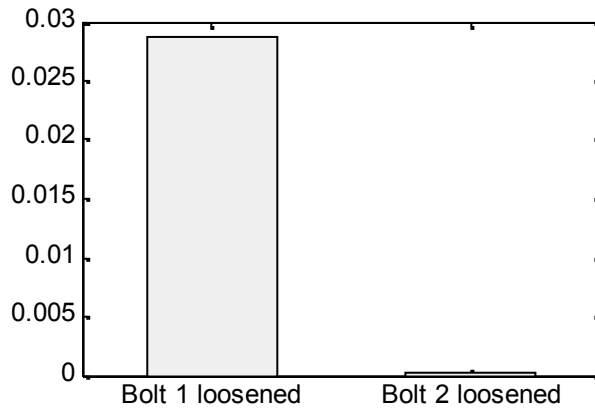


Figure 6.6 RMSD indices for two damaged models M2 and M3 (FE analysis)

6.3 Experimental Evaluation for Bolted Connection

In order to evaluate the feasibility of the FE analysis, experiment on a bolted connection is performed. Experimental setup of the bolted connection is shown in Fig. 6.1. Three damage scenarios correspondent to the FE models are carried out. The reference state is that all bolts are fastened to 160 N.m. In damage case 1, Bolt 1 is loosened by 35 N.m. To simulate damage 2, Bolt 1 is refastened to 160 N.m before loosening Bolt 2 by 35 N.m. EM impedance signatures of bolted connection in the healthy state and the two damaged states are shown in Figs. 6.7 and 6.8. As shown in Fig. 6.7, the impedance signatures between the undamaged case and damage case 1 are quite different. Meanwhile, as shown in Fig. 6.8, the impedance signature almost does not change since damage 2 occurs. To quantify the changes in impedance signatures for two damage cases, RMSD indices are calculated as shown in Fig. 6.9. The RMSD index for damage 1 is much larger than that for damage 2. Therefore, loosening Bolt 2 almost does not affect the impedance signature. A similar saying is that the impedance signature is much sensitive to loosening the bolt at the interface washer, but less sensitive to loosening the neighbor bolts.

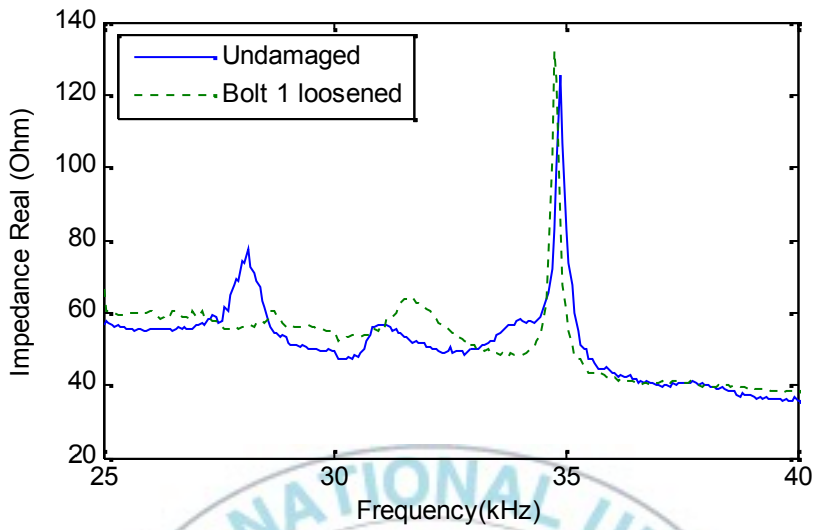


Figure 6.7 Experimental impedance signatures for undamaged and Bolt 1 loosened states

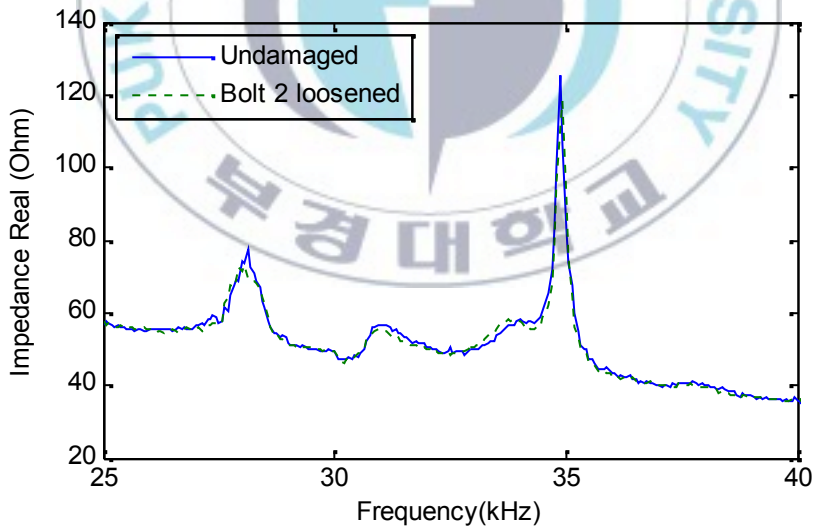


Figure 6.8 Experimental impedance signatures for undamaged and Bolt 2 loosened states

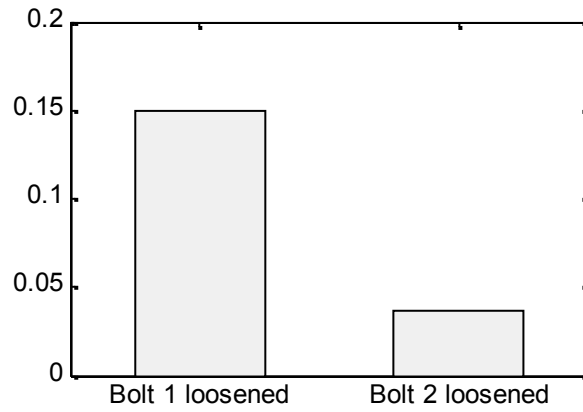


Figure 6.9 RMSD indices for two damaged cases (Experiment)



CHAPTER 7 CONCLUSION

In this study, an FE analysis of EM impedance response in damaged structural connection via high-performance interface washer was performed. The following approaches were implemented to achieve the objective. Firstly, an interface washer equipped with a piezoelectric material was designed to monitor the changes in stress fields. Secondly, an FE model of structural connection such as cable anchor connection and bolted connection was established. In the FE analysis, the interface washer was modeled to represent the changes in stress fields on the connection by using impedance-based method. Also, the effects of material and geometrical properties of the interface washer on EM impedance signature were examined to aim at designing the optimal interface washer. Thirdly, the feasibility of the FE analysis was validated by experiments on a lab-scale cable anchor connection and a bolted connection.

From the experiment and FE analysis, the following conclusions have been made.

- (1) The FE analysis of EM impedance for the simple models as free-free beam and cantilever beam were successfully established. The impedance signatures by FE analysis were well matched with experimental ones, within 40 kHz frequency range, both in trends and in resonance frequencies.
- (2) The numerical impedance signatures of cable-anchor connection model presented successfully the patterns of changes in impedance amplitude and in RMSD indices when anchor force reduced. However, the FE analysis failed to reflect the tendency of resonance frequency change due to the loss of anchor force.
- (3) Through the FE model of cable-anchor connection, the sensitivity of impedance signature to compressive anchor force loss was insignificantly affected by Young's modulus and mass

density of interface washer material. It was also found that the sensitivity of EM impedance signature to anchor force loss increased since the thickness of interface washer was reduced.

- (4) Through the FE model of bolted connection, the interface washer was found sensitive for monitoring the bolt at which the interface washer was installed. Meanwhile, the loosening of neighbor bolts did not much affect to impedance response from the PZT patch on the interface washer.

For future study, the following subjects are remained. To reflect more accurately the effect of compressive force on EM impedance signature, the interaction between the interface washer and the other elements (e.g., anchor plate, anchorage) due to change in compressive force should be considered by using FE method. Secondly, the effects of other parameters of interface washer as well as piezoelectric material need to be investigated for optimal design of interface washer. These parameters could be geometrical shape of interface washer; location, size and type of piezoelectric material. Thirdly, a method of prediction of compressive force change based on EM impedance signature needs to be studied.

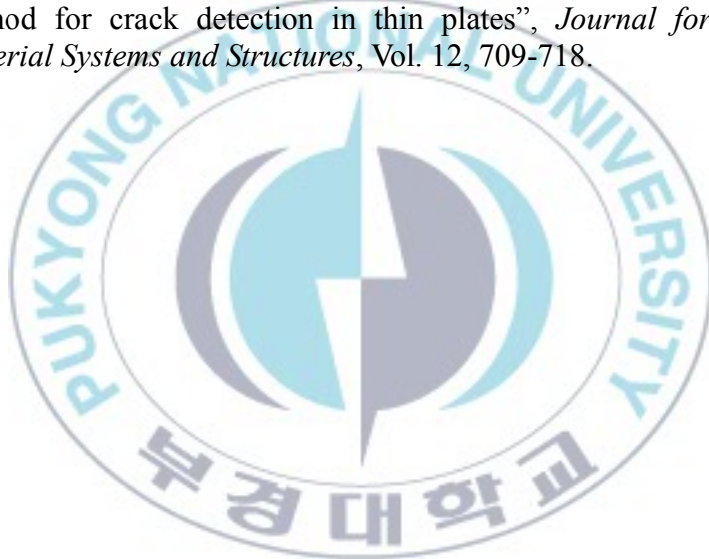
REFERENCES

- Ayres, J. W., Lalande, F., Chaudhry, Z., and Roger, C.A. (1998), “Qualitative impedance-based health monitoring of civil infrastructures”, *Smart Materials and Structures*, Vol. 7, 599-605.
- Bhalla, S. and Soh, C. K. (2003), “Structural Impedance Based Damage Diagnosis by Piezo-Transducers”, *Earthquake Engineering and Structural Dynamics*, Vol. 32(12), 1897-1916.
- COMSOL, Inc. (2010), <http://www.comsol.com>
- Efunda, Inc. (2010), <http://www.efunda.com>
- Fasel, T.R., Sohn, H., Park, G. and Farrar, C.R. (2005), “Active Sensing using Impedance-based ARX Models and Extreme Value Statistics for Damage Detection”, *Earthquake Eng. and Struc. Dynamics*, Vol. 34, 763-785.
- Giurgiutiu, V. and Zagrai, A. (2002), “Embedded self-sensing piezoelectric active sensors for on-line structural identification”, *Journal of Vibration and Acoustics*, Vol. 124, 116-125.
- Kim, J.T., Na, W.B., Park, J.H. and Hong, D.S. (2006a), “Hybrid Health Monitoring of Structural Joints using Modal Parameters and EMI Signatures”, *Proceeding of SPIE*. San Diego.
- Kim, J.T., Na, W.B., Hong, D.S., Park, J.H. (2006b), “Global and Local Health Monitoring of Plate-Girder Bridges under Uncertain Temperature Conditions”, *International Journal of Steel Structures*, Vol. 6, 369-376.
- Kim, J.T., Park, J.H., Hong, D.S., and Na, W.B. (2008), “Hybrid Damage Monitoring Scheme of PSC Girder Bridges using Acceleration and Impedance Signature”, *Journal of Korean Society of Civil Engineers (Korean)*, Vol. 28(1A), 135-146.
- Kim, J.T., Park, J.H., Hong, D.S., Cho, H.M., Na, W.B., and Yi, J.H. (2009), “Vibration and Impedance Monitoring for Prestress-Loss Prediction in PSC Girder Bridges”, *Smart Structures and Systems*, Vol. 5(1), 81-94.

- Kim, J.T., Park, J.H., Hong, D.S., and Park, W.S. (2010), "Hybrid health monitoring of prestressed concrete girder bridges by sequential vibration-impedance approaches", *Engineering Structures*, Vol. 32, 115-12.
- Kim, J.T., Park, J.H., and Hong, D.S. (2011), "Sensitivity Analysis of Impedance Sensor Node for Structural Health Monitoring in Cable-Anchor Systems", *Advanced Science Letters*, In Press.
- Koh, Y.L., Rajic, N., Chiu, W.K., and Galea, S. (1999), "Smart structure for composite repair", *Composite Structures*, Vol. 47, 745-752.
- Lam, H.F., Ko, J.M. and Wong, C.W. (1998), "Localization of Damaged Structural Connections based on Experimental Modal and Sensitivity Analysis", *Journal of Sound and Vibration*, Vol. 210(1), 91-115.
- Liang, C., Sun, F.P., and Rogers, C.A. (1996), "Electro-Mechanical Impedance Modeling of Active Material Systems", *Smart Materials and Structures*, Vol. 5(2), 171-186.
- Mascarenas, D. L. (2006), "Development of an impedance-based wireless sensor node for monitoring of bolted joint preload", *MS Thesis*, Department of Structural Engineering, University of California, San Diego.
- Mascarenas, D. L., Todd, M.D., Park, G., and Farrar, C.R. (2007), "Development of an Impedance-based Wireless Sensor Node for Structural Health Monitoring", *Smart Materials and Structures*, Vol. 16, 2137-2145.
- Park, S., Yun, C.B. and Roh, Y. (2005), "PZT-induced Lamb Waves and Pattern Recognitions for On-line Health Monitoring of Joint Steel Plates", *Proc. of SPIE*, San Diego.
- Park, S., Ahmad, S., Yun, C.B., and Roh, Y. (2006), "Multiple crack detection of concrete structures using impedance-based structural health monitoring techniques", *Experimental Mechanics*, Vol. 46(5), 609-618.

- Park, G., Cudney, H. H., and Inman, D. J. (2001), "Feasibility of using impedance-based damage assessment for pipeline structures", *Earthquake Engineering and Structural Dynamics*, Vol. 30, 1463-1474.
- Park, G., Sohn, H., Farrar, C., and Inman, D. (2003), "Overview of piezoelectric impedance-based health monitoring and path forward", *The Shock and Vibration Digest*, Vol. 35(6), 451-463.
- Park, J.H., Kim, J.T., Hong, D.S., Mascarenas, D. and Lynch, J.P. (2010a), "Autonomous smart sensor nodes for global and local damage detection of prestressed concrete bridges based on accelerations and impedance measurements", *Smart Structures and Systems*, Vol. 6, 711-730.
- Park, J.H., Lee, S.Y., and Kim, J.T. (2010b), "Development of Acceleration-PZT Impedance Hybrid Sensor Nodes Embedding Damage Identification Algorithm for PSC Girder", *Journal of Korean Society of Ocean Engineers*, Vol. 24(3), 1-10.
- Park, J.H., Hong, D.S., Kim, J.T., Na, W.B., and Cho, H.M. (2010c), "A Study on Applicability of Wireless Impedance Sensor Nodes Technique for Tensile Force Monitoring of Structural Cables", *Journal of Korean Society of Steel Construction (Korean)*, Vol. 22(1), 21-31.
- Park, J.H., Nguyen, K.D., and Kim, J.T. (2011), "Wireless Impedance Sensor Node and Interface Washer for Damage Monitoring in Structural Connections", *Advances in Structural Engineering*, In Press.
- Soh, C. K., Tseng, K. K., Bhalla, S., and Gupta, A. (2000), "Performance of smart piezoceramic patches in health monitoring for a RC bridge", *Smart Materials and Structures*, Vol. 5, 171-186.
- Sun, F. P., Chaudhry, Z., Roger, C. A., and Majmundar, M. (1995), "Automated real-time structure health monitoring via signature pattern recognition", *SPIE North American Conference on Smart Structures and Materials*, San Diego, CA.
- Tseng, K. K. and Wang, L. (2005), "Impedance-based method for nondestructive damage identification", *Journal of Engineering Mechanics*, Vol. 131(1), 58-64.

- Tseng, K. K., and Naidu, A. S. K. (2002), “Non-parametric damage detection and characterization using smart piezoelectric material”, *Smart Materials and Structures*, Vol. 11, 317-329.
- Yang, YW, Hu YH, and Lu Y. (2008), “Sensitivity of PZT impedance Sensors for damage detection of concrete structures”, *Sensors*, Vol. 8, 327-346.
- Yun, C.B., Yi, J.H. and Bahng, E.Y. (2001), “Joint Damage Assessment of Framed Structures using Neural Networks Technique”, *Engineering Structures*, Vol. 23(5), 425-435.
- Zagrai, A. N., and Giurgiutiu, V. (2001), “Electro-mechanical impedance method for crack detection in thin plates”, *Journal for Intelligent Material Systems and Structures*, Vol. 12, 709-718.



ACKNOWLEDGEMENTS

First of all, I would like to express my gratefulness to my advisor, Prof. Jeong-Tae Kim, for giving me the opportunity to study and to work in Smart Structures Engineering Laboratory (SSeL), Pukyong National University, Busan, Korea. Also, I am very grateful for his patient advice and useful comments to my research during the time I was doing my Master course here.

I would like to thank to Prof. Yeon-Sun Ryu, Prof. Won-Bae Na, Prof. Yun-Tae Kim, and Dr. Hyun-Man Cho for giving me the valuable lectures. I earned myself plenty of knowledge from their interesting topics. I also would like to thank to all professors in Department of Ocean Engineering, Pukyong National University, Korea, for their kind helps during my Master course here.

I would like to give special thanks to Dr. Jae-Hyung Park. With his kind and patient guidance, I learned so much on impedance-based method, wireless sensor node, and programming for MATLAB and C language. For those, I am very grateful. I would like to thank to Mr. Dong-Soo Hong and Mr. Po-Yong Lee for their helps on the experimental tests. I would like to thank to Mr. Duc-Duy Ho for his introducing and promoting me to SSeL. Also, I am grateful for his helps on my work and living in Korea. I would like to thank to Ms. Soyoung Lee, Ms. Sora Lee, and Ms. Dong-Ja Yang for helping me to do many research reports by Korean. To all of you, thanks for giving the pleasant time in Korea.

I would like to thank to the Brain Korean 21 program, Korea, for their financial support during my study in Department of Ocean Engineering, Pukyong National University, Korea.

Most importantly, I would like to express my gratitude to my parents who have tried their best for me. Their love, unwavering support and encouragement have made this work enable.